Published in final edited form as:
Geochim Cosmochim Acta. 2016 October 15; 191: 118–138. doi:10.1016/j.gca.2016.07.011.

Magnesium and ^{54}Cr isotope compositions of carbonaceous chondrite chondrules – Insights into early disk processes

Mia B. Olsen, **Daniel Wielandt**, **Martin Schiller**, **Elishevah M.M.E. Van Kooten**, and **Martin Bizzarro**[*]
Centre for Star and Planet Formation, Natural History Museum of Denmark, University of Copenhagen, Øster Voldgade 5-7, DK-1350, Denmark

Abstract

We report on the petrology, magnesium isotopes and mass-independent $^{54}Cr/^{52}Cr$ compositions ($\mu^{54}Cr$) of 42 chondrules from CV (Vigarano and NWA 3118) and CR (NWA 6043, NWA 801 and LAP 02342) chondrites. All sampled chondrules are classified as type IA or type IAB, have low $^{27}Al/^{24}Mg$ ratios (0.04–0.27) and display little or no evidence for secondary alteration processes. The CV and CR chondrules show variable $^{25}Mg/^{24}Mg$ and $^{26}Mg/^{24}Mg$ values corresponding to a range of mass-dependent fractionation of ~500 ppm (parts per million) per atomic mass unit. This mass-dependent Mg isotope fractionation is interpreted as reflecting Mg isotope heterogeneity of the chondrule precursors and not the result of secondary alteration or volatility-controlled processes during chondrule formation. The CV and CR chondrule populations studied here are characterized by systematic deficits in the mass-independent component of ^{26}Mg ($\mu^{26}Mg^*$) relative to the solar value defined by CI chondrites, which we interpret as reflecting formation from precursor material with a reduced initial abundance of ^{26}Al compared to the canonical $^{26}Al/^{27}Al$ of ~5×10^{-5}. Model initial $^{26}Al/^{27}Al$ values of CV and CR chondrules vary from $(1.5 \pm 4.0) \times 10^{-6}$ to $(2.2 \pm 0.4) \times 10^{-5}$. The CV chondrules display significant $\mu^{54}Cr$ variability, defining a range of compositions that is comparable to that observed for inner Solar System primitive and differentiated meteorites. In contrast, CR chondrites are characterized by a narrower range of $\mu^{54}Cr$ values restricted to compositions typically observed for bulk carbonaceous chondrites. Collectively, these observations suggest that the CV chondrules formed from precursors that originated in various regions of the protoplanetary disk and were then transported to the accretion region of the CV parent asteroid whereas CR chondrule predominantly formed from precursor with carbonaceous chondrite-like $\mu^{54}Cr$ signatures. The observed $\mu^{54}Cr$ variability in chondrules from CV and CR chondrites suggest that the matrix and chondrules did not necessarily formed from the same reservoir. The coupled $\mu^{26}Mg^*$ and $\mu^{54}Cr$ systematics of CR chondrules establishes that these objects formed from a thermally unprocessed and ^{26}Al-poor source reservoir distinct from most inner Solar System asteroids and planetary bodies, possibly located beyond the orbits of the gas giants. In contrast, a large fraction of the CV chondrules plot on the inner Solar System correlation line, indicating that these objects predominantly formed from thermally-processed, ^{26}Al-bearing precursor material akin to that of inner Solar System solids, asteroids and planets.

[*]Corresponding author. bizzarro@snm.ku.dk (M. Bizzarro).

Keywords

Carbonaceous chondrites; Chondrules; Magnesium; Chromium; Isotopes; Protoplanetary disk; Mass transport

1 Introduction

Chondritic meteorites are sedimentary rocks that represent fragments of undifferentiated asteroids that accreted during the first few million years of Solar System formation and are chemically similar to the non-volatile composition of the Sun (Wood, 1988). Thus, these primitive asteroidal bodies provide direct information on the formation and earliest evolution of the Sun and its protoplanetary disk. The major constituent of most chondrites are chondrules, millimeter-sized inclusions that were once molten in the protoplanetary disk and accumulated in the disk mid-plane together with several other kinds of particles, including low temperature components. Chondrules are mainly composed of olivine and pyroxene minerals, which crystallized within minutes to days between ~1300 and ~1800 K (Scott, 2007). These silicate minerals are also the main constituents of the fine-grained matrix that mantles chondrules and other chondritic inclusions and fills the space between them in chondrites (Scott and Krot, 2005). Chondrite meteorites and, by extension, their chondrules and matrix are believed to represent the building blocks of rocky planets. Therefore, the collisional growth of submicron dust particles into macroscopic chondrules represents the first step of planet formation in protoplanetary disks.

Judging by their sheer abundance in chondrite meteorites, chondrules must reflect one of the most energetic processes that operated in the early Solar System. Several heat sources have been proposed for the thermal processing of chondrule precursors, including shock waves (Boss and Graham, 1993; Connolly and Love, 1998; Hood, 1998; Connolly et al., 2006), current sheets (Joung et al., 2004), x-winds (Shu et al., 1997), magnetized disk winds (Salmeron and Ireland, 2012) and colliding planetesimals (Asphaug et al., 2011; Sanders and Scott, 2012). Based on the short-lived ^{26}Al-^{26}Mg chronometer (half-life of 730,000 years), it has long been accepted that chondrule formation began ~2 Myr after condensation of the Solar Systems first solids, calcium-aluminum-rich inclusions, CAIs (MacPherson et al., 1995; Kurahashi et al., 2008; Villeneuve et al., 2009; Kita and Ushikubo, 2012). However, a recent absolute chronology of chondrules based on U-corrected Pb–Pb dating, indicates formation ages ranging from 4567.32 ± 0.42 to 4564.71 ± 0.30 Myr (Connelly et al., 2012) for chondrules from Allende and NWA 5697 chondrites. These data refute the long-held view of an age gap between CAIs and chondrules and, instead, establish that chondrule formation started contemporaneously with CAIs and lasted ~3 Myr. Therefore, chondrules represent time sequenced samples that allow us to probe the nature and isotopic evolution of the material that accreted to form asteroids and, ultimately, planetary bodies.

Large-scale nucleosynthetic isotopic heterogeneity exists among inner Solar System solids, planets, and asteroids, most noticeably for neutron-rich isotopes of the iron-group elements such as, for example, ^{48}Ca, ^{50}Ti, ^{54}Cr and ^{62}Ni (Papanastassiou and Brigham, 1989; Thrane et al., 2008; Holst et al., 2013; Trinquier et al., 2007, 2009; Larsen et al., 2011; Regelous et

al., 2008; Schiller et al., 2015a). This variability is interpreted as reflecting un-mixing of nucleosynthetic components during the earliest stages of Solar System formation (Trinquier et al., 2009; Schiller et al., 2015a). Thus, variations in the abundance of stable nuclides such as ^{54}Cr within the inner Solar System can be used to track genetic relationships between early-formed solids and their respective reservoirs. Based on a limited dataset, Trinquier et al. (2009) identified correlated ^{46}Ti and ^{50}Ti nucleosynthetic variability in chondrules from the Allende CV3 chondrite, defining both excesses and deficits compared to the terrestrial composition. Similarly, Connelly et al. (2012) documented ^{54}Cr variability in individual Allende chondrules as well as chondrules from the NWA 5697 ordinary chondrite. At face value, these results indicate that chondrules formed from isotopically heterogeneous precursor material. Chondrule formation thus occurred in different regions of the protoplanetary disk prior to the transport of these objects to the accretion regions of their respective parent bodies. As such, unraveling the extent of nucleosynthetic isotope heterogeneity within chondrule populations is critical to understand whether these objects regulate the level of isotope heterogeneity observed among the inner Solar System asteroidal and planetary bodies.

Recent high-precision Mg isotope measurements of inner Solar System materials demonstrate the existence of variability in the mass-independent ^{26}Mg composition (μ^{26}Mg*) of bulk Solar System reservoirs with solar or near-solar Al/Mg ratios, which has been interpreted as reflecting heterogeneity in the initial abundance of ^{26}Al (^{26}Al decays to ^{26}Mg with a half life of ~730,000 years) across the solar protoplanetary disk at the time of CAI formation (Larsen et al., 2011). This interpretation has been challenged in some recent studies (Kita and Ushikubo, 2012; Wasserburg et al., 2012; Kita et al., 2013), arguing that the μ^{26}Mg* variability predominately reflects Mg isotope heterogeneity. In spite of this debate, an important observation is that the μ^{26}Mg* variability identified by Larsen et al. (2011) resonate with excesses and deficits in ^{54}Cr for the same samples or reservoirs. Correlated variability for nuclides of distinct nucleosynthetic origins has been interpreted as reflecting selective thermal processing of diverse presolar components (Trinquier et al., 2009; Paton et al., 2013). Thus, linking the μ^{26}Mg* and μ^{54}Cr compositions of individual chondrules may allow us to probe the scale of the correlated variability defined by bulk Solar System reservoirs. Moreover, the ^{25}Mg/^{24}Mg and ^{26}Mg/^{24}Mg ratios can be fractionated in a predictable manner during condensation and evaporation processes in the solar protoplanetary disk. As such, coupled magnesium isotope and μ^{54}Cr measurements of individual chondrules can be used to identify genetic relationships between early formed solids and asteroidal bodies as well as track the formation history of chondrule precursors.

In this paper, we report the petrology and mineral chemistry as well as the Mg and Cr isotope compositions of 42 chondrules from various CR2 and CV3 chondrites. CR chondrites are considered as one of the most primitive classes of meteorites, having experienced only mild aqueous alteration and no evidence for significant effects of thermal metamorphism (Briani et al., 2013). Our samples of CR chondrites include the LAP 02342, NWA 801 and NWA 6043 chondrites, whereas we focused on Vigarano (reduced CV3) and NWA 3118 (oxidized CV3) for our analysis of CV chondrites. Raman spectroscopy of included organic matter indicates that Vigarano is among the most pristine CV3 chondrites (Bonal et al., 2006). In contrast, the NWA 3118 oxidized CV3 apparently experienced some

degree of thermal metamorphism, although it is believed to have been less intense than for Allende (Ghimire et al., 2012). Our results indicate that chondrules from both CR and CV chondrites record significant heterogeneity in their magnesium and chromium isotope compositions. We discuss the implications of these results for understanding the origin of nucleosynthetic isotope heterogeneity among inner Solar System bodies, outward mass transport in the protoplanetary disk, and chondrule formation models.

2 Samples and Methods

Polished sections of the selected meteorites were imaged and studied using a Phillips XL40 scanning electron microscope (SEM) located at the Geological Survey of Denmark and Greenland. Our objective during the initial characterization was to select chondrules of diverse petrological textures that have largely avoided secondary alteration. Moreover, care was taken to avoid the potential presence of relic CAI material in individual chondrules, as this may result in overprinting the isotopic signature of the chondrule precursors due to the existence of large isotopic anomalies in CAIs. Based on this initial characterization, a total of 42 suitable chondrules were identified and selected for isotopic study, namely ten from Vigarano (reduced CV3), nine form NWA 3118 (oxidized CV3), ten from NWA 6043 (CR2), ten from NWA 801 (CR2) and three from LAP 02342 (CR2). The chemical composition of the major mineral phases (olivine and pyroxene) of the selected individual chondrules was analyzed using the JEOL JXA 8200 electron microprobe at University of Copenhagen, operated at 15 kV accelerating voltage, 15 nA beam current, and fully focused 4 μm beam using five wavelength spectrometers. Elemental corrections were calculated based on a mixture of natural and synthetic standards.

Following the mineralogical and chemical characterization, individual chondrules were sampled for bulk isotopic investigation using a computer assisted New Wave micro-drill using 560 microns tungsten-carbide drill bits. Approximately 6000 μg of material was sampled yielding between ~200 and 1500 μg of Mg and ~1000 ng of Cr. Drill holes were typically less than 200 microns in depth to avoid sampling matrix material. After sampling, each hole was carefully examined using a microscope to ensure that only chondrule material was sampled. The sampled material was carefully transferred into a Savilex beaker and dissolved with mixtures of concentrated HF and 7 M HNO_3 at 130 °C for one day, and subsequently dried down and then taken up again in aqua regia and heated at 130 °C for the same amount of time to ensure complete dissolution of the samples. A 5% aliquot of the individual sample dissolutions was retained for measurements of the $^{27}Al/^{24}Mg$ ratios using the Thermo X-Series quadrupole ICPMS at the Centre for Star and Planet Formation in Copenhagen and are accurate to 2%.

The remaining 95% aliquots of each sample were processed by ion exchange chromatography for Mg and Cr purification. The Mg was purified using a six steps procedure fully described in Bizzarro et al. (2011). The Cr-rich cut retrieved from step 2 of the Mg separation scheme outlined in Bizzarro et al. (2011) was further processed for Cr purification. In detail, the Cr-rich separate was first pre-treated with 200 μl 0.125 M HNO_3 0.1% H_2O_2 at 40 °C for two days. This solution was subsequently loaded on a 250 μl AG50-X8 200–400 resin bed in a five cm long column. Contaminants such as Na, K and V were

eluted from the resin with 4.5 ml 0.125 M HNO_3. Residual Fe, Ti and V were further eluted in additional 100 µl 1 M HF. A pure Cr separate was subsequently eluted from the resin bed with 1 ml of 6 M HCl. The first two washes were analyzed for Cr and reprocessed if they contained ⩾ 10% of the total Cr. Finally, the Cr samples were treated repeatedly with HNO_3 and H_2O_2 in order to minimize the presence of organics that can interfere with the isotopic analyses. Total procedural blanks were less than 1 ng and negligible compared to the typical amount of Cr processed through the purification protocol (~1000 ng).

The Mg isotope composition of chondrules was determined on the ThermoFischer Neptune Plus multiple collector inductively coupled plasma source mass spectrometer (MC-ICPMS) at the Centre for Star and Planet Formation (University of Copenhagen) using the sample-standard bracketing technique and based on methods described in Bizzarro et al. (2011). Samples were introduced in the plasma source by means of an Apex IR desolvating nebuliser in a 2% HNO_3 solution and Mg isotope data were acquired in static mode using three Faraday collectors connected to amplifiers with 10^{11} (^{25}Mg and ^{26}Mg) and 10^{10} (^{24}Mg) Ohm feedback resistors. Measurements were made in medium resolution corresponding to an effective resolving power of 2500 (M/ΔM). Samples and standards were analyzed with a signal intensity of at least 100V on mass ^{24}Mg while ensuring that the intensity of the samples and standards were matched to better than 5%. Each sample was systematically analyzed 10 times. Sample analysis comprised a total of 630 s of baseline measurements (obtained on peak) and 1667 s of data acquisition (100 scans integrated over 16.67 s).

The reference material typically used in Mg isotope studies is the DSM-3 standard (Galy et al., 2003; Young & Galy, 2004). However, DSM-3 is isotopically heavier than the Bulk Silicate Earth (BSE) by ~150 ppm, which suggests that this standard has been fractionated during the purification process (Bizzarro et al., 2011). Thus, to minimize potential inaccuracies in the mass bias corrected $^{26}Mg/^{24}Mg$ ratios resulting from inappropriate correction of the natural mass-dependent fractionation of the reference standard (Olsen et al., 2013), we elected to use a reference material more representative of BSE, namely the DTS-2b rock standard. We dissolved a large amount of DTS-2b and purified the Mg from four aliquots of this dissolution using our chemical purification scheme. The DTS-2b aliquots were first analyzed against DSM-3 to ensure that their compositions were identical to earlier studies (Table 1), and then combined and used as reference material for the analysis of unknowns.

The stable Mg-isotope ratios are reported as relative deviations from the DTS-2b reference material in the µ notation, which reflects per 1,000,000 deviations from the standard. The mass-independent component in ^{26}Mg ($\mu^{26}Mg^*$) is reported in the same fashion, but represents deviations from the internally normalized $^{26}Mg/^{24}Mg$ of the sample from the reference standard, normalized to $^{25}Mg/^{24}Mg = 0.126896$ (Bizzarro et al., 2011) using the exponential mass fractionation law. Each sample was analyzed ten times and the reported $\mu^{26}Mg^*$ and $\mu^{25}Mg$ values reflect the weighted means of the 10 analyses and associated standard error (2SE). The accuracy and external reproducibility of our data was verified by repeated analyses of terrestrial synthetic and rock standards and is estimated to be 2.5 and 20 ppm for the $\mu^{26}Mg^*$ and $\mu^{25}Mg$ values, respectively.

The Cr isotopic composition was determined on the ThermoFischer Triton thermal ionization mass spectrometer (TIMS) at the Centre for Star and Planet Formation (University of Copenhagen) on ~250 or 500 ng of Cr loaded on pre-outgassed Re-filaments with silica gel, boric acid and Al, based on protocols outlined in Trinquier et al. (2008). The samples and standards were dissolved and loaded in ~6 M HCl to ensure formation of Cr-chloride complexes. Prior to loading, each filament was heated to ~1.2 amp and dabbed with parafilm to form brackets of melted plastic that minimized spreading of the sample and loading slurry. We first loaded and dried down the equivalent of ~15 μg of silica gel, 5 μg of boron and 1 μg of Al in a mixed slurry before adding the 250 or 500 ng of sample/standard Cr. Once the sample solution was evaporated, we briefly heated the filament to ~2 amps in order to burn off the parafilm brackets and residual organics from the chemical separation procedure.

During analysis, the samples were manually or automatically heated with peak-centering and focusing to reach analyzing conditions over the course of ~20 min. Cr was then measured in static mode with a beam current of 5 or 10 V on ^{52}Cr until filament exhaustion, which was typically reached after 2–10 h. Each block of data consisted of 25 cycles of 4s integrations followed by 50 s of baseline measurements with a pre-baseline wait of 5 s to allow for signal decay in the amplifiers. Filament and lens focusing was performed every ten blocks, and isobaric interferences were corrected by monitoring ^{49}Ti, ^{51}V and ^{56}Fe. ^{49}Ti was measured with a 10^{12} Ohm amplifier while ^{51}V and ^{56}Fe were measured with 10^{11} Ohm amplifiers; given the isotopic ratio abundances of the possible interfering elements, this provided the optimal noise propagation characteristics. We never observed significant ^{49}Ti or ^{51}V beams, while ^{56}Fe was <10 mV.

The data were reduced offline using either Excel or the freely distributed Iolite data reduction package, which runs within Igor Pro (Paton et al., 2011). The reported ^{54}Cr variations represent the offset of the chondrule data to that of the average composition of the terrestrial Cr standard SRM 979 measured within the same session as the chondrules and expressed in the μ notation (per 1,000,000 deviations from the standard). The Excel data reduction used the simple average of the bracketing standards, while the Iolite data reduction utilized automatic splining to maximize the predictive power of the standard dataset (Paton et al., 2011), often resulting in a simple linear fit with time as would be expected in case of long term linear drift of the amplifiers experienced during the longest 2–3 week analytical sessions. The accuracy and external reproducibility of the μ^{54}Cr data was estimated through repeated analyses of the SRM 979 standard and the terrestrial rock standard DTS-2b within individual sessions. The μ^{54}Cr data obtained for the SRM 979 standard in three different analytical sessions are presented in Fig. 1. Five separate digestions of the DTS-2b dunite standard yielded an average μ^{54}Cr value of 1 ± 11 ppm (Van Kooten et al., 2016), indistinguishable from the pure SRM 979 standard. Based on these experiments, we estimate a conservative external reproducibility of ~20 ppm for our μ^{54}Cr data. There was no apparent difference in reproducibility between the 250 and 500 ng loads and the 5 V and 10 V methods.

3 Results

3.1 Petrology

Our sample suite is comprised of 42 chondrules sampling a range of CV3 and CR2 chondrites, 19 from two CV3 chondrites and 23 from three CR2 chondrites (Table 2). The mineral chemistry of major phases is reported for selected chondrules in Tables 3–5. Based on the fayalite (Fa) contents of the olivine composition (Table 3) and the X-ray elemental maps of sampled chondrules (Fig. 2), they can be classified into two petrographic groups, namely type IA or IAB chondrules (Hewins, 1997). Type I chondrules are those with magnesian olivine and/or low-Ca pyroxene containing less than 10 mol% fayalite (Fa) or ferrosilite. The chondrules can be further subdivided into olivine-rich, designated as A (olivine > 80%), or B for pyroxene-rich (pyroxene > 80%), whereas intermediate compositions are termed as AB. Another classification is focused on the texture of the chondrules; these range from the most common porphyritic texture, to barred, granular and radiating textures. In this study, only chondrules with porphyritic and barred textures were large enough for isotopic studies and, thus, we limited our analysis to these types of objects. Two chondrules (CV3, CV4) are compound chondrules, consisting of chondrules with both barred and porphyritic textures. Finally, secondary alteration of the chondrules is an important factor in the selection of the chondrules as the degree of alteration may impact the significance of the isotope systematics. Therefore, no heavily altered chondrules were sampled in this study and the chondrules selected for analyses were classified into three subgroups (light, moderate and intermediate) based on the amount of alteration observed by the chondrule inferred from on the amount of sulfides present, cracks in and around the chondrules as well as assessment of petrology. The majority of chondrules are characterized by porphyritic textures (33 total, 13 CV3, 20 CR2) whereas only a few had barred textures. Furthermore, the most common type sampled were IAB (28 total, 13, CV3, 15 CR2) with fourteen being type IA chondrules. The petrological information for individual chondrules is summarized in Table 2.

3.2 Magnesium isotopes

The Mg isotopic composition of the CV and CR chondrules as well as the terrestrial rock standards analyzed here are reported relative to the DTS-2b composition in Table 6. Chondrules from CV chondrites have μ^{25}Mg values ranging from −276 ± 15 to 201 ± 31, corresponding to an average and standard deviation (2sd) of 2 and 212, respectively. The CR chondrules show a somewhat more restricted range of μ^{25}Mg values, with compositions varying from −92 ± 5 to 275 ± 16. The average and standard deviation of the CR chondrules corresponds to 39 and 177, respectively. The documented μ^{25}Mg variability is much greater than the inferred external reproducibility of 20 ppm for this value (μ^{25}Mg) and confirms the presence of mass dependent Mg isotope fractionation in chondrules, in agreement with earlier studies (Galy et al., 2000; Bizzarro et al., 2004; Gounelle et al., 2007; Olsen et al., 2013; Bouvier et al., 2013). For both the CR and CV chondrule populations, it is apparent that the mode of the distribution is centered on a μ^{25}Mg value of ~0, which corresponds to the BSE value as defined by Earth's mantle (Fig. 3). There is no apparent correlation between the Mg stable isotope composition and the texture and/or mineral compositions of individual chondrules. For example, porphyritic and barred olivine chondrules span a similar

range of μ^{25}Mg values (i.e. from ca. −200 to 200), irrespective of their mineral compositions. Moreover, we find no clear trend in our data supporting a relationship between the stable isotope composition and the degree of secondary alteration of individual chondrules as suggested by Bouvier et al. (2013).

The CV and CR chondrules define comparable ^{27}Al/^{24}Mg ratios ranging from ~0.04 to ~0.27, although the average of the CV population is marginally higher (0.13) than the solar value of 0.09781 (Paton et al., 2012) compared to the near-solar average composition defined by the CR chondrules (0.10). The μ^{26}Mg* values recorded by CV chondrites range from −8.2 ± 1.6 to 5.6 ± 1.7 ppm whereas the CR chondrules have compositions that vary from −15.9 ± 1.9 to −5.7 ± 2.5 ppm. The range of μ^{26}Mg* defined by each population corresponds to ~10 ppm, demonstrating the existence of clearly resolvable μ^{26}Mg* variability among the two chondrule populations given the external reproducibility of 2.5 ppm of our measurements (Bizzarro et al., 2011). It is apparent from Fig. 4 that individual CV and CR chondrules define two distinct populations with nearly no overlap, corresponding to average μ^{26}Mg* values of −1.3 ± 5.2 (2sd) and −8.9 ± 5.5 (2sd) for the CV and CR populations, respectively. In the ^{26}Al-^{26}Mg isochron diagram, there is no clear correlation between the ^{27}Al/^{24}Mg and μ^{26}Mg* values (Fig. 5). In fact, the majority of chondrules do not fall within the compositional field predicted from a homogenous distribution of ^{26}Al and Mg isotopes in the early Solar System, requiring ^{26}Al and/or Mg isotope heterogeneity. We note that the μ^{26}Mg* compositions of CR and CV chondrules with solar or near-solar ^{27}Al/^{24}Mg values analyzed here fall between the solar value of 4.5 ± 1.0 ppm defined by CI chondrites and the Solar System's initial Mg isotope composition of −15.9 ± 1.4 ppm recorded by the combined CAI and amoeboid olivine aggregate (AOA) isochron of Larsen et al. (2011). This observation indicates that individual chondrules record a similar level of μ^{26}Mg* heterogeneity as that defined by bulk inner Solar System reservoirs (Larsen et al., 2011).

3.3 μ^{54}Cr systematics

The μ^{54}Cr values of the chondrules analyzed in this study are reported in Table 6 and shown graphically in Fig. 6. The CV chondrules record significant ^{54}Cr variability, defining μ^{54}Cr values ranging from −79 to 201 ppm. This compositional range is comparable to that defined by inner Solar System asteroidal and planetary bodies, which have μ^{54}Cr values varying from −108 ± 25 ppm in the ureilite parent body to 169 ± 9 ppm for the CI chondrite parent body (Trinquier et al., 2007; Yamakawa et al., 2010; Qin et al., 2010; Larsen et al., 2011). In contrast, CR chondrules record a much more restricted range of μ^{54}Cr values, varying from 121 to 166 ppm (Fig. 6). At face value, this observation suggests that the CR chondrule precursors were predominantly derived from the accretion regions of primitive carbonaceous chondrites (CM, CR and CI) whereas the precursor material of CV chondrules may have originated in various regions of the inner protoplanetary disk, namely from the accretion regions of terrestrial planets and differentiated asteroids to the accretion regions of carbonaceous chondrites. The modes of the CR and CV chondrule distributions are comparable to the bulk μ^{54}Cr compositions defined by the respective chondrites (Fig. 6). Finally, we note that for both CR and CV populations, some chondrules record μ^{54}Cr values

greater than that defined by the most primitive carbonaceous chondrites, namely CI chondrites.

4 Discussion

4.1 Origin of μ^{25}Mg isotope heterogeneity

The Mg stable isotope variability we report for chondrules from Vigarano and NWA 3118 compares favorably with that documented by earlier studies of CV chondrules obtained using similar techniques (Galy et al., 2000; Bizzarro et al., 2004), although the range of μ^{25}Mg values reported here is more restricted. However, we note that the bulk of the Mg stable isotope variability reported in earlier work is defined by Al-rich chondrules, which display μ^{25}Mg values that are up to ~2610 ppm heavier than the solar μ^{25}Mg value defined by CI chondrites. However, the majority of Al-rich chondrules are believed to represent CAI and ferromagnesian chondrule hybrids (Russell et al., 2005) such that their stable Mg isotope compositions are likely to be controlled by the CAI component as these typically record heavy Mg. Limiting our comparison to chondrules with $^{27}Al/^{24}Mg$ ratios similar to that observed in our CV population (i.e. less than ca. 0.3) restricts the range of μ^{25}Mg values to less than ~700 ppm in earlier studies of CV chondrules (Galy et al., 2000; Bizzarro et al., 2004), which is in better agreement with our data. Bouvier et al. (2013) recently reported Mg stable isotope compositions of a number of chondrules from the Murchison and Murray CM2 carbonaceous chondrites. These authors report μ^{25}Mg values ranging from −538 to 532 ppm relative to the DTS-2b composition, which represent a greater degree of μ^{25}Mg variability compared to CV and CR chondrules. They suggest that the observed μ^{25}Mg variability in CM chondrules reflects the combined effects of both aqueous alteration and volatility-controlled processes such evaporation and/or condensation during chondrule formation.

Care was taken in selecting the chondrules analyzed here to avoid any potential bias of the isotope signals from secondary alteration occurring during fluid-assisted metaphorphism on the CR and CV parent bodies. As such, most of chondrules we selected contain little or no evidence for secondary alteration. Bouvier et al. (2013) suggested that the least altered chondrules from CM2 chondrites record, on average, isotopically lighter magnesium isotope compositions compared to the heavily altered chondrules. Such a systematic offset is not apparent in our dataset, indicating that the observed μ^{25}Mg variability in CV and CR chondrules does not reflect secondary alteration processes on the parent asteroid. Olsen et al. (2013) recently reported high-precision data for chondrules from the Hammadah al Hamra 237 CBb chondrites. Similar to Gounelle et al. (2007), the data of Olsen et al. (2013) show that the μ^{25}Mg values of individual chondrules are positively correlated to their $^{27}Al/^{24}Mg$ ratios. This observation clearly demonstrates that the μ^{25}Mg variability in CBb chondrules is controlled by volatility-related processes, supporting the origin of these chondrules from a plume produced by a large-scale asteroidal collision (Krot et al., 2005). Therefore, the recognition of correlated variability between $^{27}Al/^{24}Mg$ and μ^{25}Mg values in a chondrule population implies Mg-isotope fractionation by evaporation and/or condensation processes during the chondrule-forming event. Similar to the CM chondrule population reported by Bouvier et al. (2013), the CV and CR chondrule populations analyzed here do not show

Europe PMC Funders Author Manuscripts

correlated μ^{25}Mg and ^{27}Al/^{24}Mg variability (Fig. 7). Although it is possible that the lack of correlation reflects a complex history of the chondrules involving multiple evaporation and condensation events, we explore below alternative scenarios that can account for the observed μ^{25}Mg variability if unrelated to chondrule-forming processes.

High temperature processing of dust associated with transient heating events during the earliest evolutionary stages of the protoplanetary disk can lead to stable isotope fractionation of Mg through evaporation and condensation processes. Indeed, refractory material such as CAIs and AOAs typically record highly fractionated Mg isotope compositions ranging from μ^{25}Mg values of ~−2000 ppm in some AOAs to enrichments as high as ~10,000 ppm per atomic mass unit (AMU) in type B CAIs (Larsen et al., 2011). Moreover, enrichments in heavy Mg on the order of 2–4% per AMU are commonly observed in CAIs with Fractionation and Unidentified Nuclear isotope effects (FUN CAIs). Transport and admixing of thermally processed dust in the formation regions of chondrule precursors provides an efficient means of generating μ^{25}Mg variability in chondrules. Thus, the μ^{25}Mg variability observed among CV and CR chondrule populations can be understood as reflecting stable Mg-isotope heterogeneity of the chondrule precursors.

4.2 Origin of μ^{26}Mg* deficits

The CV and CR chondrule populations studied here are characterized by systematic deficits in μ^{26}Mg* relative to the solar value of 4.5 ± 1.0 defined by CI chondrites (Larsen et al., 2011). The magnitude of the μ^{26}Mg* deficits are not correlated to the ^{27}Al/^{24}Mg values, indicating the presence of μ^{26}Mg* variability unrelated to ^{26}Al decay. Indeed, in the ^{26}Al-^{26}Mg isochron diagram (Fig. 5), the majority of chondrules record ^{26}Al–^{26}Mg systematics that are apparently not compatible with the hypothesis of ^{26}Al homogeneity. Deficits in μ^{26}Mg* can result from ^{26}Al and/or Mg isotope heterogeneity or, alternatively, complex prehistory of the chondrule precursors. For example, it is possible to imagine scenarios in which a chondrule with near solar Al/Mg can be characterized by a deficit in μ^{26}Mg* in the model of ^{26}Al homogeneity via significant Al/Mg fractionation events during its history. Indeed, if a chondrule is formed from an Al-free reservoir at the time of Solar System formation, it will develop a deficit of −38 ppm relative to the chondritic composition. Adding Al to this object after decay of ^{26}Al to increase its Al/Mg close to the solar value would then result in an object characterized by a μ^{26}Mg* deficit and solar Al/Mg ratio. We submit this class of models to account for the μ^{26}Mg* observed in the majority of chondrules violates our basic understanding of chondrule formation processes. Both theory and experiments predict limited Al/Mg fractionation during chondrule formation processes (i.e. Desch et al., 2012) such that little variety is expected in the Al/Mg ratios of chondrules, which is consistent with our dataset. In contrast, if Al/Mg fractionation was a common process associated with chondrule formation, significant variability would be expected and this is clearly not observed. Thus, we conclude that a complex history of chondrules and/or their precursors involving multiple Al/Mg fractionation events cannot account for the μ^{26}Mg* deficits recorded by most chondrules and, as such, we consider ^{26}Al and/or Mg-isotope heterogeneity as the main cause of the observed μ^{26}Mg* deficits.

Our results demonstrate that Mg isotope measurements of early Solar System material cannot be used to infer ^{26}Al homogeneity as attempted by Villeneuve et al. (2009). Instead, distinguishing between ^{26}Al and Mg-isotope heterogeneity require careful comparison between the ^{26}Al–^{26}Mg and uranium-corrected Pb–Pb ages of objects with simple thermal histories. Using this approach, Schiller et al. (2015b) recently provided a detailed comparison of the U-corrected Pb–Pb and internal ^{26}Al–^{26}Mg isochron ages for three rapidly-cooled angrite meteorites. Their results demonstrate that the ^{26}Al-^{26}Mg ages obtained for angrites are systematically younger by ~1.5 Myr relative to their absolute ages, establishing that the angrite parent body accreted from precursor material typified by a reduced initial abundance of ^{26}Al relative to the canonical ratio. The three angrites concordantly define an initial ^{26}Al/^{27}Al of $1.33^{+0.21}_{-0.18} \times 10^{-5}$ for the precursor of their parent body, which is identical to that inferred from the μ^{26}Mg* compositions of young angrites of $1.61 \pm 0.32 \times 10^{-5}$ (Larsen et al., 2011). This observation is consistent with the proposal that the bulk of the Solar System's μ^{26}Mg* variability reflects ^{26}Al heterogeneity (Larsen et al., 2011). Initial disk ^{26}Al heterogeneity is also consistent with the inferred variability in initial ^{26}Al/^{27}Al for early-formed solar system condensates, including FUN CAIs and hibonite-bearing CAIs in CM chondrites (Hsu et al., 2011; Holst et al., 2013). Thus, similarly to Schiller et al. (2015b), we interpret the deficits in μ^{26}Mg* observed in chondrules as reflecting formation from precursor material characterized by a reduced initial abundance of ^{26}Al relative to the canonical value.

The range of μ^{26}Mg* values recorded by individual chondrules ranges from the solar value down to the initial composition of the Solar System defined by Efremovka CAIs and AOAs and, thus, can be fully accounted for by ^{26}Al heterogeneity and does not require Mg isotope heterogeneity. This interpretation is further strengthened by the homogeneous distribution of silicon isotopes in bulk Solar System reservoirs, which suggest limited Mg heterogeneity as Mg and Si are synthesized by similar nucleosynthetic processes (Pringle et al., 2013). Thus, if the totality of the μ^{26}Mg* variability is related to ^{26}Al heterogeneity, it is possible to estimate the initial ^{26}Al abundance in the chondrule precursors by comparing their present-day μ^{26}Mg* with the initial μ^{26}Mg* defined by the Efremovka CAI-AOA isochron and its intercept at the solar ^{27}Al/^{24}Mg ratio. The initial ^{26}Al/^{27}Al is defined by a model 2 point isochron of the Solar System initial μ^{26}Mg* of −16 and the chondrule present-day μ^{26}Mg* composition. Using this approach and limiting our analysis to chondrules with ^{27}Al/^{24}Mg ratios within 10% of the solar value, we calculate initial ^{26}Al/^{27}Al values in CR and CV precursors ranging from $(1.5 \pm 4.0) \times 10^{-6}$ to $(2.2 \pm 0.4) \times 10^{-5}$ (Table 7). The three CV chondrules with near-solar ^{27}Al/^{24}Mg ratios are characterized by systematically higher initial ^{26}Al/^{27}Al values compared to the corresponding subset of seven CR chondrules, suggesting a lower initial abundance of ^{26}Al in the accretion regions of CR chondrules. This observation is consistent with the initial ^{26}Al/^{27}Al ratios in CR chondrules determined by internal isochron relationships, which are among the lowest observed in chondrules (Nagashima et al., 2014).

4.3 μ^{54}Cr variability and the Solar System's μ^{54}Cr–μ^{26}Mg* correlation line

The presence of isotope heterogeneity of nucleosynthetic origin among bulk Solar System reservoirs provides a means of probing genetic relationships between early formed solids,

asteroids and planetary bodies. In particular, significant $\mu^{54}Cr$ variability exists between carbonaceous chondrite groups and meteorites originating from asteroidal bodies believed to have formed in the accretion regions of terrestrial planets such as ordinary and enstatite chondrites and the majority of differentiated meteorites. Bulk carbonaceous chondrites are characterized by excesses in $\mu^{54}Cr$ ranging from +57 ± 11 to +156 ± 6 ppm relative to the terrestrial composition (Trinquier et al., 2007). In contrast, enstatite and ordinary chondrites as well as Mars, the Moon and most differentiated meteorites record $\mu^{54}Cr$ values that span from the terrestrial composition to deficits of ~100 ppm. Thus, carbonaceous chondrites have apparently sampled, on average, material formed in a distinct reservoir in the terms of their $\mu^{54}Cr$ composition compared to the enstatite and ordinary chondrite population. Dynamical models for the early evolution of the Solar System suggest that the asteroid belt was first depleted by the passage of the giant planets but then repopulated by planetesimals following the final outward migration of Jupiter (Walsh et al., 2011). In this scenario, enstatite and ordinary chondrites represent samples of asteroids that formed within the orbit of Jupiter whereas the parent asteroids of carbonaceous chondrites reflect bodies that formed between and beyond the accretion regions of the giant planets (Morbidelli et al., 2012). Accretion of the carbonaceous chondrites beyond the snow line is in accord with the much higher water content of these meteorites (Robert and Epstein, 1982; Kerridge, 1985) compared to that of enstatite and ordinary chondrites (McNaughton et al., 1981; Robert et al., 1987; Hutson and Ruzicka, 2000). The dichotomy in ^{54}Cr composition observed between carbonaceous and noncarbonaceous material is also mirrored by a number of other nuclides, including ^{43}Ca, ^{48}Ca, ^{46}Ti, ^{50}Ti, ^{62}Ni and ^{88}Sr (Regelous et al., 2008; Trinquier et al., 2009; Paton et al., 2013; Schiller et al., 2015a). These observations have been used to speculate that the isotopic dichotomy reflects a fundamental difference in the accretion regions of the precursor material, namely that the carbonaceous material formed beyond the snow line whereas the noncarbonaceous material originated Sunward of the snow line (Warren, 2011; Larsen et al., 2016). Another possibility is that the observed isotopic diversity reflects time (i.e. Jacquet et al., 2012), implying a fundamental difference in the composition of the material that accreted to form asteroidal bodies during the lifetime of the protoplanetary disk. However, two lines of evidence suggest that time alone cannot account for the isotopic dichotomy observed between carbonaceous and other types of chondrites. First, individual chondrules for which both Pb–Pb ages and ^{54}Cr compositions are available indicate the existence of a ^{54}Cr-poor reservoir akin to the composition of differentiated asteroids (ureilites, eucrites and angrites) and Mars for the first Myr of the Solar System (Connelly et al., 2012). Second, CM, CI and CR chondrites record comparable accretion ages based on their ^{53}Mn–^{53}Cr sysmatics (Sugiura and Fujiya, 2014) – yet, CR have a distinct ^{54}Cr–$^{26}Mg^*$ signature relative to CI and CM chondrites suggesting a fundamental difference in the nature of their precursors (Van Kooten et al., 2016). Collectively, these observations suggest that the ^{54}Cr variability can be used as a fingerprint to differentiate between material formed beyond the snow line compared to material originating from accretion regions of the terrestrial planets (Warren, 2011) and, thus, we discuss below the implications of this interpretation.

The CV chondrules record $\mu^{54}Cr$ values that range from −79 to +201 ppm and, thus, define a range of compositions that is comparable to asteroidal and planetary bodies from the inner

Solar System. At face value, this observation suggests that CV chondrites comprise chondrules formed from precursors that originated at various orbital distances, namely from the accretion regions of most differentiated asteroids and terrestrial planets to the formation regions of carbonaceous chondrites. In accord with the presence of refractory inclusions formed close to the young Sun in CV chondrites (Krot et al., 2009), the occurrence of chondrules with inner Solar System μ^{54}Cr signatures in these chondrites require efficient lateral outward transport of material during the earliest stages of the evolution of the solar protoplanetary disk. In contrast to CV chondrules, CR chondrules define a much more restricted range of μ^{54}Cr values characterized by compositions found in bulk carbonaceous chondrites. This observation suggests that CR chondrules formed from precursors predominantly formed in the accretion region of their parent body, with little input of material with inner Solar System μ^{54}Cr signatures. This is consistent with the low abundance of CAIs in CR chondrites thereby supporting the view of limited transport of inner Solar System solids to their accretion region. The presence of chondrules with μ^{54}Cr excesses greater than that observed in bulk CI chondrites in both the CV and CR populations suggest the existence of highly primitive material in their accretion regions.

In the inner Solar System, bulk planetary materials with solar or near-solar ^{27}Al/^{24}Mg ratios record positively correlated variability in μ^{26}Mg* and μ^{54}Cr. This correlation is interpreted as reflecting progressive thermal processing of in-falling ^{26}Al-rich molecular cloud material, which resulted in preferential loss by sublimation of thermally unstable and isotopically anomalous presolar carriers, producing residual isotopic heterogeneity (Trinquier et al., 2009; Larsen et al., 2011; Paton et al., 2013; Schiller et al., 2015a). In this model, the correlated μ^{26}Mg*–μ^{54}Cr array represents the unmixing of distinct dust populations with contrasting thermal properties, namely unmixing of old, galactically-inherited homogeneous dust from a young supernovae-derived dust component formed shortly prior to or during the evolution of the giant molecular cloud structure parental to the protosolar molecular cloud core (Schiller et al., 2015a). Van Kooten et al. (2016) recently reported μ^{26}Mg* and μ^{54}Cr data for metal-rich carbonaceous chondrites (CR, CH, CB) and their components, including a number of chondrules from CR chondrites. They showed that metal-rich carbonaceous chondrites and their component do not fall on the Solar System's μ^{26}Mg*–μ^{54}Cr correlation line, but instead define a negatively correlated array extending to an end-member composition depleted in μ^{26}Mg* and enriched in μ^{54}Cr relative to CI chondrites. This composition is consistent with that expected for thermally-unprocessed primordial molecular cloud material prior to its pollution by stellar-derived ^{26}Al. As such, Van Kooten et al. (2016) interpret the μ^{26}Mg*–μ^{54}Cr signature observed in metal-rich carbonaceous chondrites as reflecting the incorporation of a significant amount of primordial molecular cloud material in their accretion region. In this model, objects accreted in the outer Solar System, namely metal-rich carbonaceous chondrites as well as Oort cloud and Jupiter family comets reflect a mixture of thermally processed, inner Solar System material radially transported to large distances together with accreting primordial ^{26}Al-free molecular cloud material. This interpretation implies the existence of a primary ^{26}Al disk heterogeneity inherited from the giant molecular cloud parental to our Solar System (see Van Kooten et al., 2016 for additional details). Our new and more extensive μ^{26}Mg* and μ^{54}Cr dataset for CR chondrules plots on the array defined by metal-rich carbonaceous chondrites, providing

additional support for the existence of admixing of primordial, ^{26}Al-poor material in the accretion regions of metal-rich carbonaceous chondrites (Fig. 8). This strengthens the idea that metal-rich carbonaceous chondrites and their components formed from precursor material distinct from the bulk of the inner Solar System, possibly from a reservoir located beyond the orbit of the gas giants. In contrast to CR chondrules, the CV chondrules investigated here fall close to the inner Solar System correlation line, suggesting that these objects predominantly formed from thermally-processed, ^{26}Al-bearing precursor material akin to that of inner Solar System solids, asteroids and planets. However, it is clear from Fig 8. That a number of CV chondrules plot towards the array defined by CR chondrules and metal-rich carbonaceous chondrites. This observation suggests admixing of minor amounts of primordial, ^{26}Alpoor molecular cloud material in the precursor material of some CV chondrules.

4.4 Implications for mass transport processes in the solar protoplanetary disk

The presence of high-temperature refractory inclusions formed near the proto-Sun in the accretion regions of carbonaceous chondrites and cometary objects requires an efficient outward transport mechanism to the outer Solar System (Krot et al., 2009). Likewise, the ~3 Myr age range defined by individual chondrules from various chondrites (Connelly et al., 2012) as well as the presence of chondrules with an inner Solar System signature in carbonaceous chondrites requires that storage and/or recycling occurred during the entire lifetime of the protoplanetary disk. Two classes of models have been invoked to explain how high temperature refractory material was redistributed throughout the disk to be incorporated into primitive bodies. One class of models are disk models that explore how the inward transport of mass and angular momentum may lead to outward transport during the final stages of the formation of the Sun. For example, it has been suggested that in viscously evolving disks, turbulence would combine with the large-scale flows of the disk to carry refractory material outward against the inward motions associated with gas drag and accretion thereby providing a means to preserve and diffuse material at larger orbital distances (Cuzzi et al., 2003; Ciesla, 2007, 2010). An important assumption in these two-dimensional models, however, is that the inward transport of mass results in the radial outward transport of angular momentum (Lynden-Bell and Pringle, 1974), which in turn may lead to outward diffusion of dust. In these models, transport of material is most efficient in highly turbulent disks, which may limit the efficiency of this mechanism to the earliest stages. If asteroidal accretion was initiated within a few 10^5 years of CAI formation as suggested by recent studies (i.e. Schiller et al., 2015b), outward diffusion via the disk midplane would result in the incorporation of refractory material within early formed asteroidal and planetary embryos. However, the paucity of CAIs in the accretion regions of Earth, Mars, most differentiated asteroids as well as ordinary and enstatite chondrites (i.e. Trinquier et al., 2009) implies that outward diffusive transport may not have been the dominant transport mechanism. A second type of models is based on the powerful magnetically-driven stellar outflows characteristic of the evolution of young stars and their disks. Both observations and numerical simulations indicate that protostars exhibit powerful outflows of material accelerated to supersonic speeds along the polar axis of the star or as winds from the disk (Bontemps et al., 1996), which, collectively, provide a means of releasing the angular momentum inherited from the accretion process. Solids may be

entrained and accelerated in jets and winds resulting in the outward transport of material in ballistic trajectories above the disk (Shu et al., 1996; Hu, 2010). Although the role of stellar outflows in the formation of chondritic components such as CAIs and chondrules is uncertain (i.e. Desch et al., 2010), disk winds and jets are a generic feature of protostars and, thus, can provide a potentially efficient mechanism for outward transport and recycling of material during the entire lifetime of the protoplanetary disk (i.e. Hansen, 2013). Accepting that stellar outflows may be the dominant mode of outward transport and recycling of solids, we explore below the implications of our chondrule data for tracking mass transport.

Recent numerical simulations suggest that the main growth phase of asteroids results from gas-drag-assisted accretion of chondrules, leading to the formation of planetary embryos within timescales of less than ~5 Myr (Johansen et al., 2015). If correct, this implies that chondrules dominate the precursor material of most asteroids and, by extension, planets. As such, these components can be used to track mass transport processes during the early evolutionary stage of the protoplanetary disk. Van Kooten et al. (2016) recently suggested that, similar to cometary objects, the parent body of CR chondrites accreted beyond the orbits of the gas giants whereas parent bodies of other carbonaceous chondrite groups accreted Sunward of the gas giants, possibly towards the outer part of the asteroid belt. As such, the chondrule populations that accreted in the CV and CR parent bodies may reflect distinct transport histories and/or processes. Chondrules from CR2 chondrites record a restricted range of μ^{54}Cr and μ^{26}Mg* values indicating derivation from an outer Solar System reservoir with little input of inner Solar System material. This observation is in accord with the scarcity of CAI material in metal-rich carbonaceous chondrites, which suggests that the outward transport of inner Solar System material to the accretion region of cometary objects may have been only possible during the early, deeplyembedded stage of the Proto-Sun characterized by powerful high-velocity jets (Bontemps et al., 1996). In contrast, approximately 50% of the chondrules in CV3 chondrites have μ^{54}Cr composition typical of inner Solar System compositions indicating significant admixing of inner Solar System material to the accretion region of the CV parent body. The high abundance of CAI material in CV chondrites relative to CR supports this observation. Thus, outward transport and recycling of inner Solar System material to the outer part of the asteroid belt may have been more protracted and, hence, driven by lower-velocity stellar and disk winds, which may have been active for the entire duration of the accretion phase of the proto-Sun (Reipurth and Bally, 2001).

4.5 Implications for chondrule formation models

Nebular shock waves are currently the favored mechanism for melting chondrule precursors. The proposed sources of shock waves include infalling clumps of dust and gas (Boss and Graham, 1993), bow shocks generated by planetary embryos (Weidenschilling et al., 1998), spiral arms and clumps in a gravitationally unstable protoplanetary disk (Boss and Durisen, 2005), and X-ray flares (Shu et al., 1996; Nakamoto et al., 2005). The complementary between the major elemental composition of the matrix and chondrules has been used to exclude separate origins and later mixing of chondrules and matrix (Hezel and Palme, 2010). In this view, matrix and chondrules from individual chondrite groups formed in the same localized region of the protoplanetary disk and, thus, are genetically related. The presence of

μ^{26}Mg* and μ^{54}Cr variability among chondrules from CR and CV chondrites confirms the existence of distinct chondrule populations in individual chondrite groups. The observed isotope variability suggests that chondrules from individual chondrite groups formed from isotopically diverse precursor material in different regions of the protoplanetary disk and were subsequently transported to the accretion regions of their respective parent bodies. This is consistent with the presence of age variability of ~3 Myr between chondrule from individual chondrites (Connelly et al., 2012), which requires transport and/storage. At face value, these data appear inconsistent with the concept of chondrule-matrix complementary as originally envisaged, namely that all chondrules from an individual chondrites are all genetically related to the coexisting matrix (i.e. Hezel and Palme, 2010; Palme et al., 2015). Recent models of evolving viscous disks, however, suggest that a complementary relationship between chondrules and dust can be preserved for long time-scales provided that the decoupling between chondrules and gas is limited (Goldberg et al., 2015). In these models, various chondrule populations remained in complementarity such that the bulk contribution from each source is chemically solar and, thus, so is the final mixture. However, these experiments assume that the main transport mechanism of chondrules occurs through outward diffusion via the disk midplane. In disk models where outward transport of material is associated with stellar outflows (i.e. Shu et al., 1996), the dust component is not expected to be efficiently coupled to the gas and, thus, it is unclear how complementary can be preserved. A possibility is the observed chondrule-matrix complementarity is an expression of the generic process of chondrule formation and does not reflect a genetic link. In this view, the matrix comprises a complement related to the chondrule formation process (Alexander, 2005) such that the bulk composition of the matrix is shifted from its starting composition and, thus, appears complementary to a chondrule composition. This does not require that the matrix is genetically linked to the chondrules in an individual chondrite but merely that some of it has experienced earlier chondrule formation events. Thus, fractions of the matrix in a particular chondrite may be complementary to chondrule populations in other chondritic meteorites. Finally, our interpretation that the ^{26}Mg*–μ^{54}Cr systematics can be linked to distinct regions of the protoplanetary disk requires that the chondrule-forming process operated at various orbital distances, namely from the inner protoplanetary disk to beyond the accretion regions of the gas giants.

A different class of models suggest that chondrules may be the product of colliding planetesimals (i.e. Sanders and Scott, 2012; Fedkin and Grossman, 2013). One model posits that, following the melting of early-accreted planetesimals by the decay of ^{26}Al, collisions led to the splashing of their liquid contents thereby producing cascades of molten droplets that would have cooled to become chondrules. A different model suggests that chondrules formed in impact-generated plumes from unmolten planetesimals of chondritic compositions. Given that planetesimal meltdown and the generation of an impact related plume will lead to isotopic homogenization, chondrules produced by impact processes are predicted to record identical μ^{54}Cr values. Alternatively, chondrules from individual chondrites may represent the products of multiple collisional events involving different planetesimals. In this model, chondrules with solar or near-solar Al/Mg ratios are expected to fall on the Solar System's μ^{26}Mg*–μ^{54}Cr correlation line, similarly to differentiated and primitive planetesimals. A fraction of the CV chondrules analysed here record variable

$\mu^{26}Mg^*$– $\mu^{54}Cr$ compositions that lie on the Solar System's line. As such, it is plausible that a fraction of the CV chondrules were formed by colliding molten planetesimals, although this requires contribution from multiple asteroidal sources. Our interpretation that the trend defined by metal-rich chondrites reflects admixing of primordial ^{26}Al-poor material (i.e. Van Kooten et al., 2016) is difficult to reconcile with formation of the CR chondrules by colliding molten planetesimals given the limited amounts of ^{26}Al available for driving planetesimal melting. Alternatively, CR chondrules could be the formed in impact-generated plumes from unmolten planetesimals of chondritic compositions. However, given the isotopic homogenization expected from the process (i.e. CB chondrules; Olsen et al., 2013), the $\mu^{26}Mg^*$–$\mu^{54}Cr$ variability defined by CR chondrules would require multiple asteroidal sources.

5 Conclusions

We have investigated the petrology and conducted high-precision $\mu^{25}Mg$, $\mu^{26}Mg^*$ and $\mu^{54}Cr$ measurements of a number of chondrules from CV and CR chondrites. The main conclusions of our study can be summarized as follows:

1. In agreement with earlier studies (Galy et al., 2000; Bizzarro et al., 2004; Bouvier et al., 2013), our subset of chondrules from CV and CR chondrites record Mg stable isotope variability characterized by both heavy and light compositions relative to Earth's mantle. The stable isotope compositions of individual chondrules are not correlated with their Al/Mg ratios or the degree of secondary alteration. We suggest that the $\mu^{25}Mg$ variability reflects Mg-isotope heterogeneity of the chondrule precursors.

2. The CV and CR chondrule populations studied here are characterized by systematic deficits in $\mu^{26}Mg^*$ relative to the solar value of 4.5 ± 1.0 ppm defined by CI chondrites (Larsen et al., 2011). The magnitude of the $\mu^{26}Mg^*$ deficits are not correlated to the $^{27}Al/^{24}Mg$ ratios. Similarly to Olsen et al. (2013), Schiller et al. (2015b) and Van Kooten et al. (2016), we interpret the $\mu^{26}Mg^*$ deficits as reflecting formation from precursor material with a reduced initial abundance of ^{26}Al compared to the canonical value of ~5×10^{-5}, defining initial $^{26}Al/^{27}Al$ values ranging from $(1.5 \pm 4.0) \times 10^{-6}$ to $(2.2 \pm 0.4) \times 10^{-5}$. The CV chondrules with near-solar $^{27}Al/^{24}Mg$ ratios are characterized by systematically higher initial $^{26}Al/^{27}Al$ values compared to the corresponding subset of CR chondrules, suggesting a lower initial abundance of ^{26}Al in the accretion regions of CR chondrules. This is consistent with the initial $^{26}Al/^{27}Al$ ratios in CR chondrules that are among the lowest observed.

3. The CV chondrules record significant variability in their $\mu^{54}Cr$ compositions, which is comparable to the variability defined by inner Solar System asteroidal and planetary bodies. This observation suggests that CV chondrules formed from isotopically diverse material at distinct orbital distances and were thereafter transported to the accretion regions of the CV parent asteroid. In contrast, CR chondrules show restricted $\mu^{54}Cr$

Europe PMC Funders Author Manuscripts

variability, which is limited to compositions typical of primitive bodies such as CR, CM and CI parent asteroids. Thus, the formation of CR chondrules occurred in a more localized disk environment relative to that of CV chondrules. Collectively, the μ^{54}Cr data for CV and CR chondrules do not support a genetic link between all chondrules and matrix within individual chondrite groups.

4. All chondrules from CR chondrites investigated here fall off the Solar System's μ^{26}Mg*–μ^{54}Cr correlation line, similarly to components (chondrules and clasts) from other metal-rich carbonaceous chondrites such as CH and CB chondrites. Collectively, all metal-rich carbonaceous chondrites define an array extending from an inner Solar System composition towards a μ^{26}Mg*-depleted and μ^{54}Cr-enriched component. This composition is consistent with that expected for thermally-unprocessed primordial molecular cloud material prior to its pollution by stellar-derived ^{26}Al. Given that high fractions of primordial molecular cloud material are expected to survive only in the outer part of the Solar System, our data are consistent with the idea that metal-rich carbonaceous chondrites and their components formed from outer Solar System material (Van Kooten et al., 2016). In contrast, a large fraction of the CV chondrules plot on the inner Solar System correlation line, indicating that these object predominantly formed from thermally-processed, ^{26}Al-bearing precursor material akin to that of inner Solar System solids, asteroids and planets. However, it is clear that a number of CV chondrules plot towards the array defined by CR chondrules and metal-rich carbonaceous chondrites, requiring the admixing of minor amounts of primordial ^{26}Al-poor molecular cloud material in their precursors.

5. The μ^{26}Mg* and μ^{54}Cr data suggest efficient recycling and transport of inner Solar System chondrules to the accretion region of the CV parent asteroid. This is in accord with the presence of abundant inner Solar System refractory material such as CAIs and AOAs in CV chondrites. In contrast, chondrules from CR chondrites record a restricted range of μ^{54}Cr and μ^{26}Mg* values indicating derivation from an outer Solar System reservoir with little input of inner Solar System material. Thus, transport of inner Solar System material may to the outer Solar System may have been limited to the early, deeply-embedded stage of the proto-Sun characterized by powerful high-velocity jets. Outward transport of inner Solar System material to the accretion region of the CV parent asteroid belt may have been more protracted and, hence, driven by lower-velocity stellar and disk winds, which may have been active for the entire duration of the accretion phase of the proto-Sun.

6. The presence of μ^{26}Mg* and μ^{54}Cr variability among chondrules from CR and CV chondrites confirms the existence of distinct chondrule populations in individual chondrite groups. The observed isotope variability suggests that chondrules from individual chondrite groups

formed from isotopically diverse precursor material in different regions of the protoplanetary disk and were subsequently transported to the accretion regions of their respective parent bodies. At face value, these data appear inconsistent with the concept of chondrule-matrix complementary as originally envisaged, namely that all chondrules from an individual chondrite are genetically related to the coexisting matrix.

Acknowledgements

Funding for this project was provided by grants from the Danish National Research Foundation (grant number DNRF97) and from the European Research Council (ERC Consolidator grant agreement 616027-STARDUST2ASTEROIDS) to M.B. We thank the associate editor Sara S. Russell and three anonymous referees for their comments, which greatly improved our paper.

References

Alexander CMO'D. Re-examining the role of chondrules in producing the elemental fractionations in chondrites. Meteorit Planet Sci. 2005; 40:943–965.

Asphaug E, Jutzi M, Movshovitz N. Chondrule formation during planetesimal accretion. Earth Planet Sci Lett. 2011; 308:369–379.

Bizzarro M, Baker JA, Haack H. Mg isotope evidence for contemporaneous formation of chondrules and refractory inclusions. Nature. 2004; 431:275–278. [PubMed: 15372023]

Bizzarro M, Paton C, Larsen KK, Schiller M, Trinquier A, Ulfbeck D. High-precision Mg-isotope measurements of terrestrial and extraterrestrial material by HR-MC-ICPMS –implications for the relative and absolute Mg-isotope composition of the bulk silicate Earth. J Anal At Spectrom. 2011; 26:565–577.

Bonal L, Quirico E, Bourot-Denise M, Montagnac G. Determination of the petrologic type of CV3 chondrites by Raman spectroscopy of included organic matter. Geochim Cosmochim Acta. 2006; 70:1849–1863.

Bontemps S, André P, Terebey S, Cabrit S. Evolution of outflow activity around low-mass embedded young stellar objects. Astron Astrophys. 1996; 311:858–872.

Bourdon B, Tipper ET, Fitoussi C, Stracke A. Chondritic Mg isotope composition of the Earth. Geochim Cosmochim Acta. 2010; 74:5069–5083.

Boss AP, Durisen RH. Chondrule-forming shock fronts in the Solar Nebula: a possible unified scenario for planet and chondrite formation. Astrophys J. 2005; 621:L137–L140.

Boss AP, Graham JA. Clumpy disk accretion and chondrule formation. Icarus. 1993; 106:168–178.

Bouvier A, Wadhwa M, Simon SB, Grossman L. Magnesium isotopic fractionation in chondrules from the Murchison and Murray CM2 carbonaceous chondrites. Meteorit Planet Sci. 2013; 48:339–353.

Briani G, Quirico E, Gounelle M, Paulhiac-Pison M, Montagnac G, Beck P, Orthous-Daunay F-R, Bonal L, Jacquet E, Kearsley A, Russell SS. Short duration thermal metamorphism in CR chondrites. Geochim Cosmochim Acta. 2013; 122:267–279.

Ciesla F. Outward transport of high-temperature materials around the mid-plane of the solar nebula. Science. 2007; 318:613–615. [PubMed: 17962555]

Ciesla F. The distributions and ages of refractory objects in the solar nebula. Icarus. 2010; 208:455–467.

Connelly JN, Bizzarro M, Krot AN, Nordlund Å, Wielandt D, Ivanova MA. The absolute chronology and thermal processing of solids in the solar protoplanetary disk. Science. 2012; 338:651–655. [PubMed: 23118187]

Connolly HC, Love SG. The formation of chondrules: petrologic tests of the shock wave model. Science. 1998; 280:62–67. [PubMed: 9525858]

Connolly, HC.; Desch, SJ.; Ash, RD.; Jones, RH. Meteorites and the Early Solar System II. Lauretta, DS.; McSween, H., editors. University Arizona; Tucson: 2006. p. 383-397.

Cuzzi JN, Davis SS, Dobrovolskis AR. Blowing in the wind. II. Creation and redistribution of refractory inclusions in a turbulent protoplanetary nebula. Icarus. 2003; 66:385–402.

Desch SJ, Morris MA, Connolly HC, Boss AP. A critical examination of the x-wind model for chondrule and calcium-rich, aluminum-rich inclusion formation and radionu-clide production. Astrophys J. 2010; 725:692–711.

Desch SJ, Morris MA, Connolly HC, Boss AP. The importance of experiments: constraints on chondrule formation models. Meteorit Planet Sci. 2012; 47:1139–1156.

Fedkin AV, Grossman L. Vapor saturation of sodium: key to unlocking the origin of chondrules. Geochim Cos-mochim Acta. 2013; 112:226–250.

Galy A, Young ED, Ash RD, O'Nions RK. The formation of chondrules at high gas pressures in the solar nebula. Science. 2000; 290:1751–1753. [PubMed: 11099410]

Galy A, Yoffe O, Janney PE, Williams RW, Cloquet C, Alard O, Halicz L, Wadhwa M, Hutcheon ID, Ramon E, Carignan J. Magnesium isotope heterogeneity of the isotopic standard SRM980 and new reference materials for magnesium-isotope-ratio measurements. J Anal At Spectrom. 2003; 18:1352–1356.

Ghimire, B.; Dall'Asen, AG.; Gerton, JM.; Ivans, II.; Bromley, BC. Raman spectroscopy investigation in the NWA 3118 meteorite: implications for planet formation. American Physical Society Meeting; 2012. Abstract #K1.035

Goldberg AZ, Owen JE, Jacquet E. Chondrule transport in protoplanetary discs. Mon Not R Astron Soc. 2015; 452:4054–4069.

Gounelle M, Young ED, Shahar A, Tonui E, Kearsley A. Magnesium isotopic constraints on the origin of CBb chondrites. Earth Planet Sci Lett. 2007; 256:521–533.

Hansen BMS. The circulation of dust in protoplanetary discs and the initial conditions of planet formation. Mon Not R Astron Soc. 2013; 440:3545–3556.

Handler MR, Baker JA, Schiller M, Bennett VC, Yaxley GM. Magnesium stable isotope composition of Earth's upper mantle. Earth Planet Sci Lett. 2009; 282:306–313.

Hewins RH. Chondrules. Annual Review of Earth and Planetary Sciences. 1997; 25:61–83.

Hezel DC, Palme H. The chemical relationship between chondrules and matrix and the chondrule–matrix complementarity. Earth Planet Sci Lett. 2010; 294:85–93.

Hood LL. Thermal processing of chondrule precursors in planetesimal bow shocks. Meteorit Planet Sci. 1998; 33:97–107.

Holst JC, Olsen MB, Paton C, Nagashima K, Schiller M, Wielandt D, Larsen KK, Connelly JN, Jørgensen JK, Krot AN, Nordlund A, et al. ^{182}Hf–^{182}W age dating of a ^{26}Al-poor inclusion and implications for the origin of short-lived radioisotopes in the Early Solar System. Proc Natl Acad Sci USA. 2013; 110:8819–8823. [PubMed: 23671077]

Hsu W, Guan Y, Wang Y. Al-Mg systematics of hibonite-bearing Ca, Al-rich inclusions from Ningqiang. Met Planet Sci. 2011; 46:719–728.

Hu R. Transport of the first rocks of the solar system by X-winds. Astrophys J. 2010; 725:1421–1428.

Hutson M, Ruzicka A. A multi-step model for the origin of E3 (enstatite) chondrites. Met Planet Sci. 2000; 35:601–608.

Jacquet E, Gounelle M, Fromang S. On the aerodynamic redistribution of chondrite components in protoplanetary disks. Icarus. 2012; 220:162–173.

Johansen A, Mac Low M-M, Lacerda P, Bizzarro M. Growth of asteroids, embryos and Kuiper belt objects by chondrule accretion. Sci Adv. 2015; 1:e1500109. [PubMed: 26601169]

Joung MR, Mac Low M-M, Ebel DS. Chondrule formation and protoplanetary disk heating by current sheets in non-ideal magnetohydrodynamic turbulence. Astrophys J. 2004; 606:532–541.

Kerridge JF. Carbon, hydrogen and nitrogen in carbonaceous meteorites: abundances and isotopic compositions in bulk samples. Geochim Cosmochim Acta. 1985; 49:1707–1714. [PubMed: 11539652]

Kita NT, Ushikubo T. Evolution of protoplanetary disk inferred from ^{26}Al chronology of individual chondrules. Meteorit Planet Sci. 2012; 47:1108–1119.

Kita NT, Yin Q-Z, MacPherson GJ, Ushikubo T, Jacobsen B, Nagashima K, Kurahashi E, Krot AN, Jacobsen SB. ^{26}Al–^{26}Mg isotope systematics of the first solids in the early solar system. Meteorit Planet Sci. 2013; 48:1383–1400.

Kurahashi E, Kita NT, Nagahara H, Morishita Y. ^{26}Al–^{26}Mg systematics of chondrules in a primitive CO chondrite. Geochim Cosmochim Acta. 2008; 72:3865–3882.

Krot AN, Amelin Y, Cassen P, Meibom A. Young chondrules in CB chondrites from a giant impact in the early solar system. Nature. 2005; 436:989–992. [PubMed: 16107841]

Krot AN, Amelin Y, Bland P, Ciesla FJ, Connelly J, Davis AM, Huss GR, Hutcheon ID, Makide K, Nagashima K, Nyquist LE, et al. Origin and chronology of chondritic components: a review. Geochim Cosmochim Acta. 2009; 73:4963–4997.

Larsen KK, Trinquier A, Paton C, Schiller M, Wielandt D, Ivanova MA, Connelly JN, Nordlund Å, Krot AN, Bizzarro M. Evidence for magnesium isotope heterogeneity in the solar protoplanetary disk. Astrophys J. 2011; 735:L37.

Larsen KK, Schiller M, Bizzarro M. Accretion timescales and style of asteroidal differentiation in an ^{26}Al-poor protoplanetary disk. Geochim Cosmochim Acta. 2016; 176:295–315. [PubMed: 27445415]

Lynden-Bell D, Pringle JE. The evolution of viscous discs and the origin of the nebular variables. Mon Not R Astron Soc. 1974; 168:603–637.

MacPherson GJ, Davis AM, Zinner E. The distribution of Aluminium-26 in the early solar system – a reappraisal. Meteoritics. 1995; 30:365–386.

McNaughton NJ, Borthwicks S, Fallick AK, Pillinger CT. D/H ratio in unequilibrated ordinary chondrites. Nature. 1981; 294:639–641.

Morbidelli A, Lunine JL, O'Brien DP, Raymond SN, Walsh KJ. Building terrestrial planets. Annu Rev Earth Planet Sci. 2012; 40:251–275.

Nagashima K, Krot AN, Huss GR. ^{26}Al in chondrules from CR2 chondrites. Geochem J. 2014; 48:561–570.

Nakamoto, T.; Hayashi, MR.; Kita, NT.; Tachibana, S. Chondrule-forming shock waves in the solar nebula by X-ray flares. Chondrites and the Protoplanetary Disk. Krot, N.; Scott, ERD.; Reipurth, B., editors. Vol. 341. 2005. p. 993-892.

Olsen MB, Schiller M, Krot AN, Bizzarro M. Magnesium isotope evidence for single stage formation of CB chondrules by colliding planetesimals. Astrophys J. 2013; 776:L1.

Palme H, Hezel DC, Ebel DS. The origin of chondrules: constraints from matrix composition and matrix-chondrule complementarity. Earth Planet Sci Lett. 2015; 411:11–19.

Papanastassiou DA, Brigham CA. The identification of meteorite inclusions with isotope anomalies. Astrophys J. 1989; 338:L37–L40.

Paton C, Hellstrom J, Paul B, Woodhead J, Hergt J. Iolite: freeware for the visualisation and processing of mass spectrometric data. J Anal At Spectrom. 2011; 26:2508–2518.

Paton C, Schiller M, Ulfbeck D, Bizzarro M. High-precision ^{27}Al/^{24}Mg ratio determination using a modified isotope-dilution approach. J Anal At Spectrom. 2012; 27:644–652.

Paton C, Schiller M, Bizzarro M. Identification of an ^{84}Sr-depleted carrier in primitive meteorites and implications for thermal processing in the solar protoplanetary disk. Astrophys J. 2013; 763:L40.

Pogge von Strandmann PAE, Elliott T, Marschall HR, Coath C, Lai Y-J, Jeffcoate AB, Ionov DA. Variations of Li and Mg isotope ratios in bulk chondrites and mantle xenoliths. Geochim Cosmochim Acta. 2011; 75:5247–5268.

Pringle EA, Savage PS, Jackson MG, Barrat J-A, Moynier F. Si isotope homogeneity of the solar nebula. Astrophys J. 2013; 779:L123.

Qin L, Alexander CMO'D, Carlson RW, Horan MF, Yokohama T. Contributors to chromium isotope variation of meteorites. Geochim Cosmochim Acta. 2010; 74:1122–1145.

Regelous M, Elliott T, Coath CD. Nickel isotope heterogeneity in the early solar system. Earth Planet Sci Lett. 2008; 272:330–338.

Reipurth B, Bally J. Herbig-haro flows: probes of early stellar evolution. Annu Rev Astron Astrophys. 2001; 39:403–455.

Russell, SS.; Krot, AN.; Huss, GR.; Keil, K.; Itoh, S.; Yurimoto, H.; MacPhersen, GJ. The genetic relationship between refractory inclusions and chondrules. Chondrites and the Protoplanetary Disk, Astron Soc Pac Conf Ser. Krot, AN.; Scott, ERD.; Reipurth, B., editors. Vol. 341. 2005. p. 317-350.

Robert F, Epstein S. The concentration of isotopic compositions of hydrogen carbon and nitrogen in carbonaceous chondrites. Geochim Cosmochim Acta. 1982; 16:81–95.

Robert FM, Javoy J, Halbout B, Dimon B, Merlivat L. Hydrogen isotopes abondances in the solar system, Part 1. Unequilibrated chondrites. Geochim Cosmochim Acta. 1987; 51:1787–1806.

Salmeron R, Ireland TR. Formation of chondrules in magnetic winds blowing through the proto-asteroid belt. Earth Planet Sci Lett. 2012; 327:61–67.

Sanders IS, Scott ERD. The origin of chondrules and chondrites: debris from low-velocity impacts between molten planetesimals. Meteorit Planet Sci. 2012; 47:2170–2192.

Scott ERD. Chondrites and the protoplanetary disk. Annu Rev Earth Planet Sci. 2007; 35:577–620.

Scott ERD, Krot AN. Thermal processing of silicate dust in the solar nebula: clues from primitive chondrite matrices. Astrophys J. 2005; 623:571–578.

Schiller M, Paton C, Bizzarro M. Evidence for nucleosynthetic enrichment of the protosolar molecular cloud core by multiple supernova events. Geochim Cosmochim Acta. 2015a; 149:88–102. [PubMed: 25684790]

Schiller M, Connelly JN, Glad AC, Mikouchi T, Bizzarro M. Early accretion of protoplanets inferred from a reduced inner solar system ^{26}Al inventory. Earth Planet Sci Lett. 2015b; 420:45–54. [PubMed: 27429474]

Shu FH, Shan H, amd Lee T. Towards an astrophysical theory of chondrites. Science. 1996; 27:1545–1552.

Shu FH, Shang H, Glassgold AE, Lee T. X-rays and fluctuating x-winds from protostars. Science. 1997; 277:1475–1479.

Sugiura N, Fujiya W. Correlated accretion ages and ε^{54}Cr of meteorite parent bodies and the evolution of the solar nebula. Meteorit Planet Sci. 2014; 49:772–787.

Thrane K, Nagashima K, Krot AN, Bizzarro M. Discovery of a new FUN CAI from a CV carbonaceous chondrite: evidence for multistage thermal processing in the protoplanetary disk. Astrophys J. 2008; 680:L141–L144.

Teng F-Z, Li W-Y, Ke S, Marty B, Dauphas N, Huang S, Wu F-Y, Pourmand A. Magnesium isotopic composition of the Earth and chondrites. Geochim Cosmochim Acta. 2010; 74:4150–4166.

Trinquier A, Birck J-L, Allègre CJ. Widespread ^{54}Cr heterogeneity in the inner solar system. Astrophys J. 2007; 655:1179.

Trinquier A, Birck J-L, Allègre C, Göpel C, Ulfbeck D. ^{53}Mn–^{53}Cr systematics of the early Solar System revisited. Geochim Cosmochim Acta. 2008; 72:5146–5163.

Trinquier A, Elliott T, Ulfbeck D, Coath C, Krot AN, Bizzarro M. Origin of nucleosynthetic isotope heterogeneity in the solar protoplanetary disk. Science. 2009; 324:374–376. [PubMed: 19372428]

Van Kooten EMM, Wielandt D, Schiller M, Nagashima K, Thomen A, Larsen KK, Olsen MB, Nordlund Å, Krot A, Bizzarro M. Isotopic evidence for primordial molecular cloud material in metal-rich carbonaceous chondrites. Proc Natl Acad Sci USA. 2016; 113:2011–2016. [PubMed: 26858438]

Villeneuve J, Chaussidon M, Libourel G. Homogeneous distribution of 26Al in the solar system from the Mg isotopic composition of chondrules. Science. 2009; 325:985–988. [PubMed: 19696348]

Walsh KJ, Morbidelli A, Raymond SN, O'Brien DP, Mandell AM. A low mass for Mars from Jupiter's early gas-driven migration. Nature. 2011; 475:206–209. [PubMed: 21642961]

Warren PH. Stable-isotopic anomalies and the accretionary assemblage of the Earth and Mars: a subordinate role for carbonaceous chondrites. Earth Planet Sci Lett. 2011; 311:93–100.

Wasserburg GJ, Wimpenny J, Yin Q-Z. Mg isotopic heterogeneity, Al-Mg isochrons, and canonical ^{26}Al/^{27}Al in the early solar system. Meteorit Planet Sci. 2012; 47:1980–1997.

Weidenschilling SJ, Marzari F, Hood LL. The origin of chondrules at jovian resonances. Science. 1998; 279:681–684. [PubMed: 9445468]

Wood JA. Chondritic meteorites and the solar nebula. Annu Rev Earth Planet Sci. 1988; 16:53–72.

Yamakawa A, Yamashita K, Makishima A, Nakamura E. Chromium isotope systematics of achondrites: Chronology and isotopic heterogeneity of the inner solar system bodies. Astrophys J. 2010; 720:150–154.

Yamashita K, Maruyama S, Yamakawa A, Nakamura E. ^{53}Mn–^{53}Cr chronometry of CB chondrite: evidence for uniform distribution of ^{53}Mn in the early solar system. Astrophys J. 2010; 723:20–24.

Young ED, Galy A. The isotope geochemistry and cosmochemistry of magnesium. Rev Mineral Geochem. 2004; 55:197–230.

Europe PMC Funders Author Manuscripts

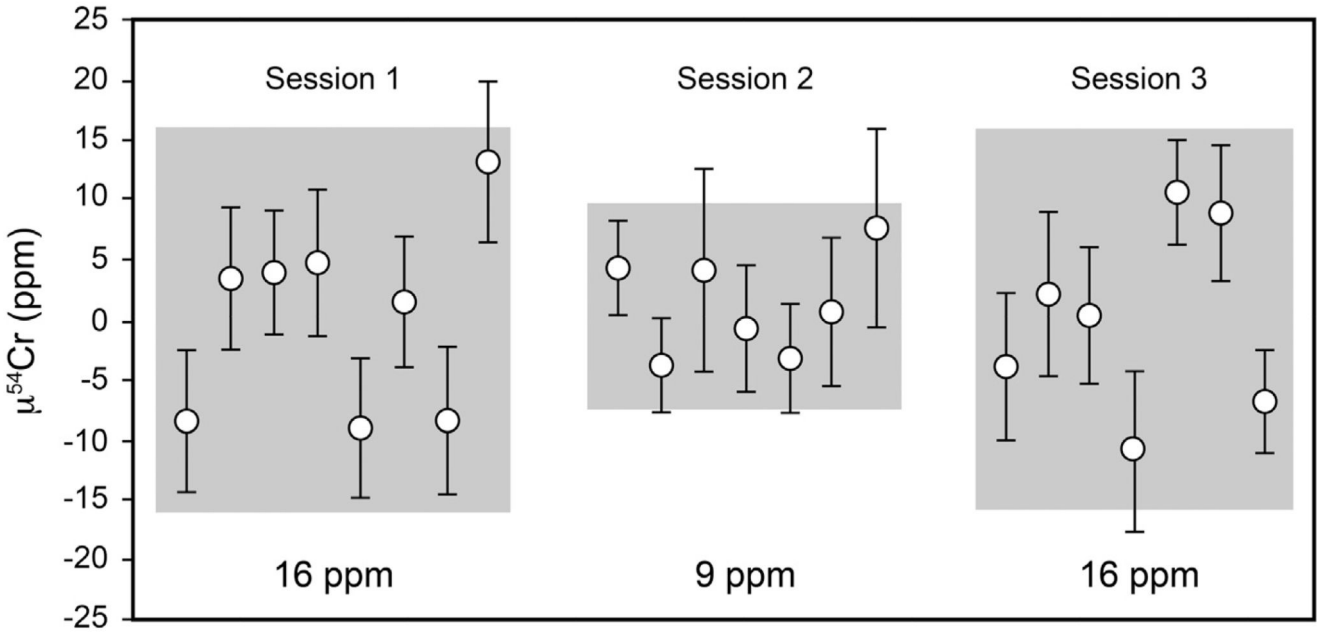

Fig. 1.

$\mu^{54}Cr$ values for the SRM 979 metal standard obtained for three different analytical sessions during the course of this study, which indicates an external reproducibility of <20 ppm for this ratio.

Europe PMC Funders Author Manuscripts

Europe PMC Funders Author Manuscripts

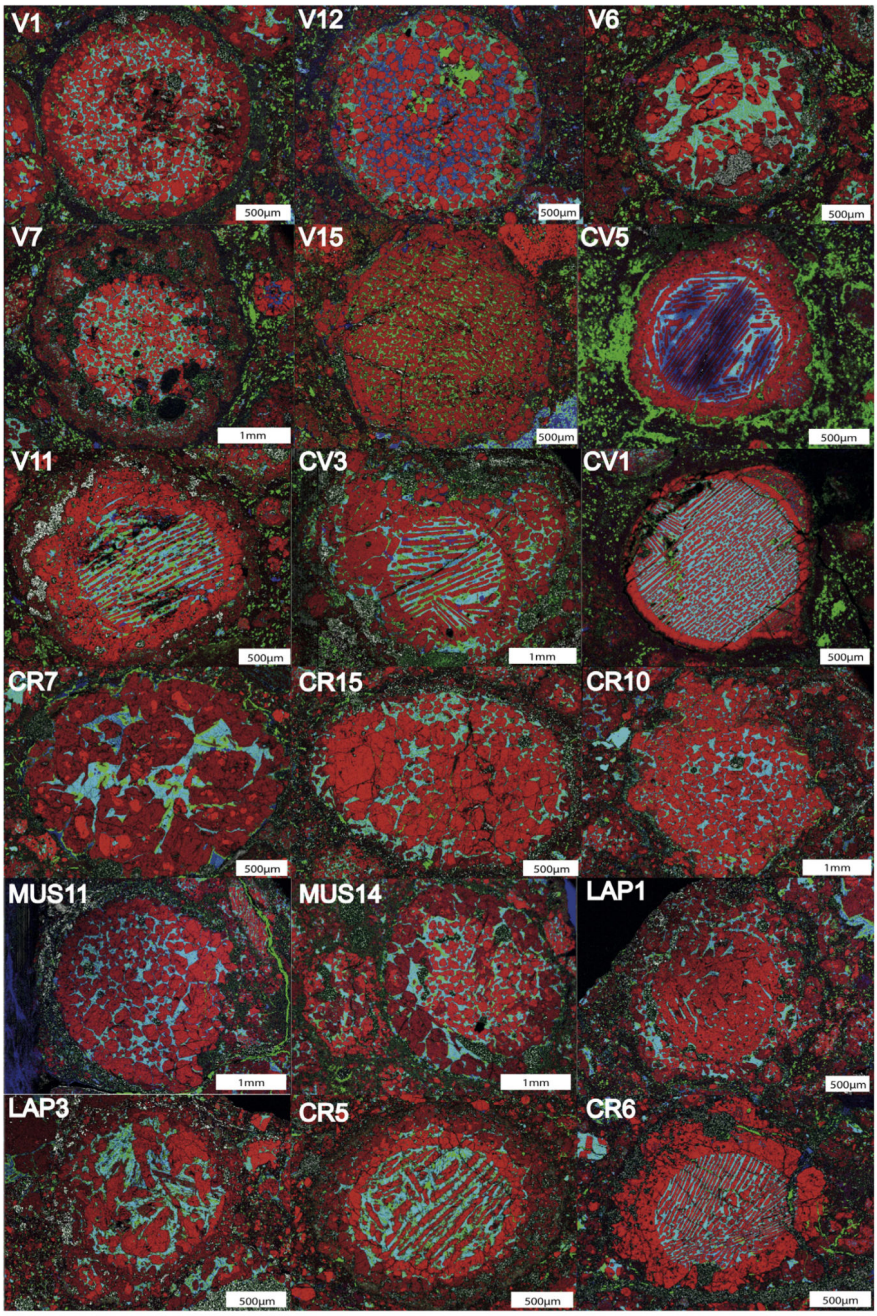

Fig. 2.

Combined Mg-Al-Ca (red-blue-green) X-ray elemental images of selected chondrules from CV3 and CR2 chondrites investigated in this study. The major mineral phases observed are olivine (red) surrounded by a mesostasis containing mainly pyroxene (green), plagioclase (blue) and for some chondrules spinel (purple). (For interpretation of the references to colour in this figure legend, the reader is referred to the web version of this article.)

Europe PMC Funders Author Manuscripts

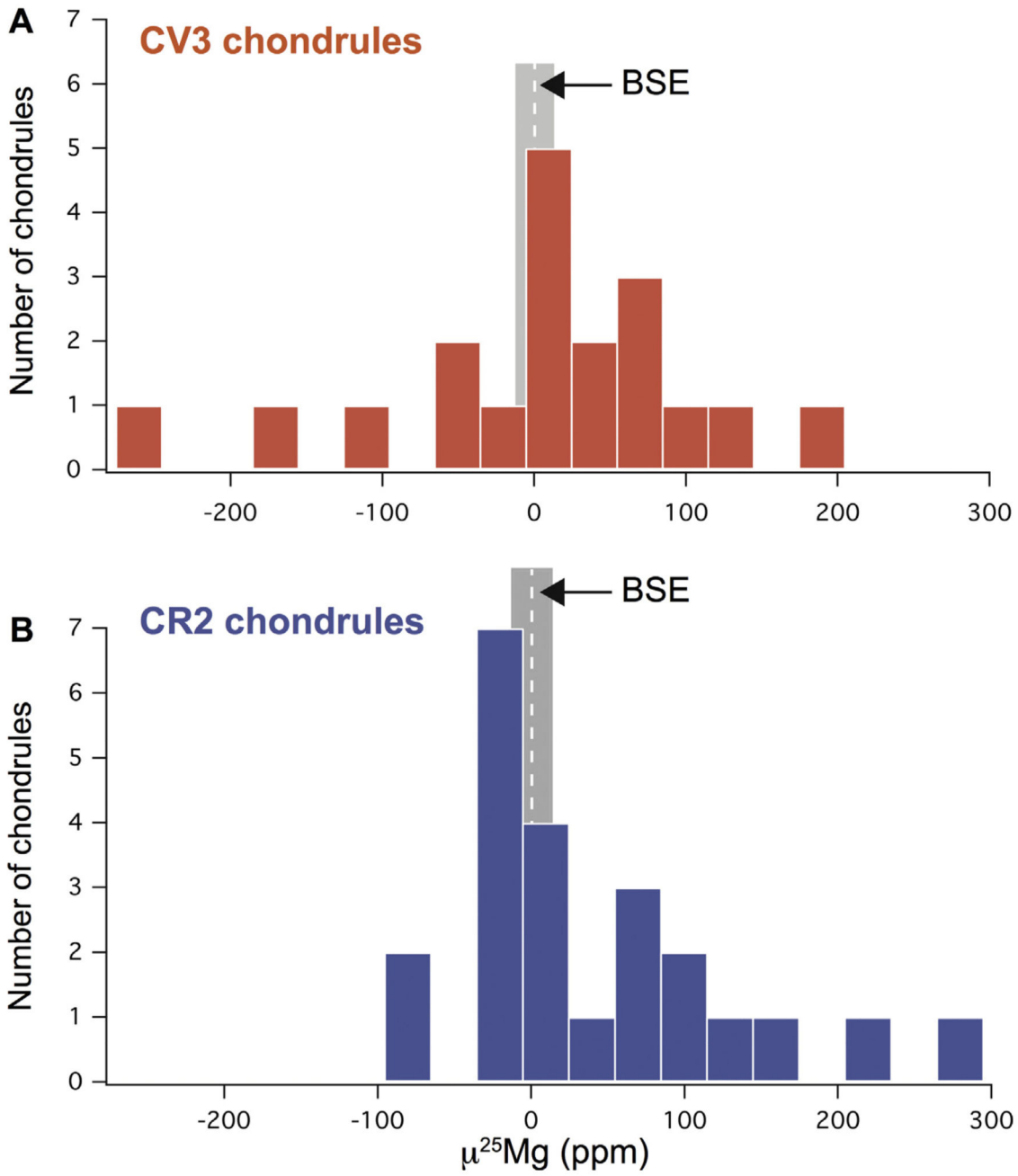

Fig. 3.

Histograms depicting the distribution of the μ^{25}Mg (ppm) values for individual chondrules from the CV3 (A) and CR2 (B) chondrites investigated in this study. The bulk Silicate Earth (BSE) value is based on multiple analyses of the international rock standard DTS-2 dunite (this study, Bizzarro et al., 2011; Olsen et al., 2013) and is in agreement with estimates reported by other groups (i.e. Handler et al., 2009; Bourdon et al., 2010; Teng et al., 2010; Pogge von Strandmann et al., 2011).

Europe PMC Funders Author Manuscripts

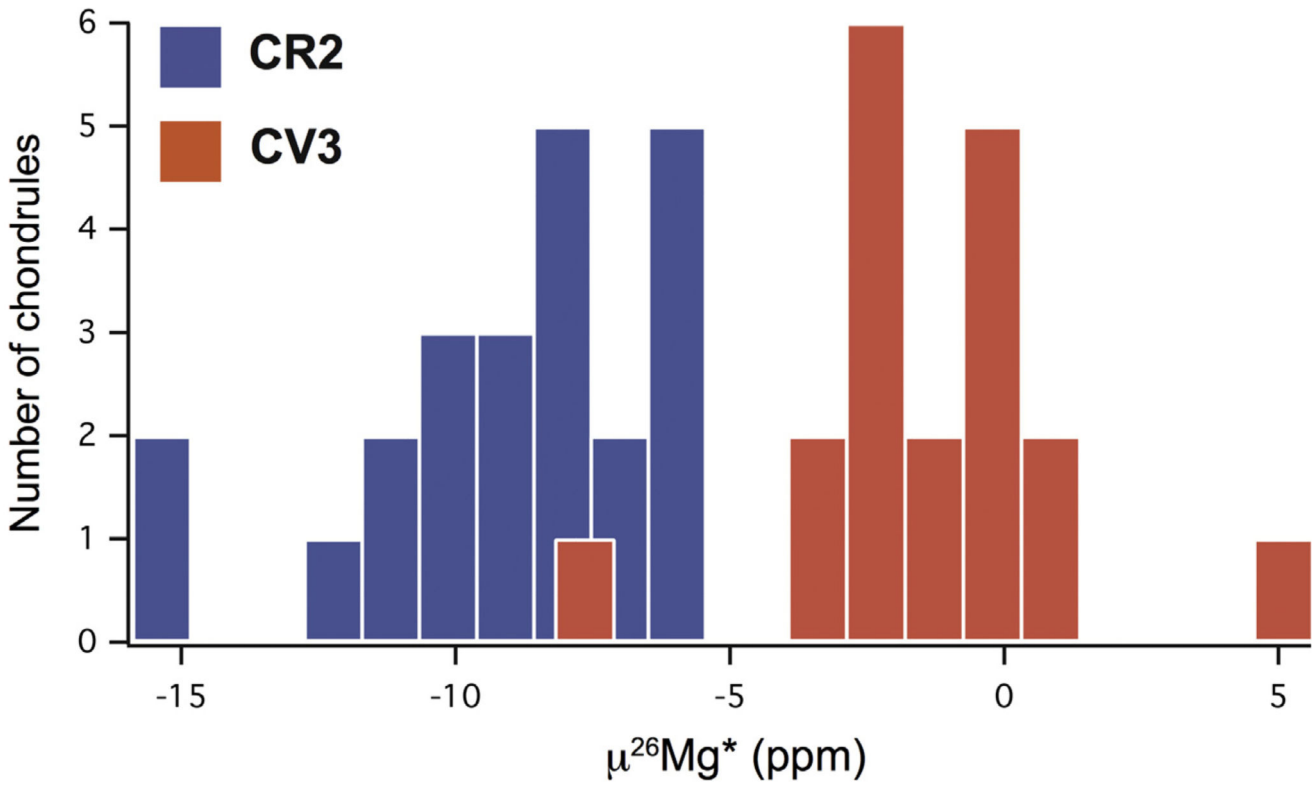

Fig. 4.

Histograms depicting the distribution of the $\mu^{26}Mg^*$ (ppm) values for individual chondrules from the CV3 (red) and CR2 (blue) chondrites investigated in this study.

Europe PMC Funders Author Manuscripts

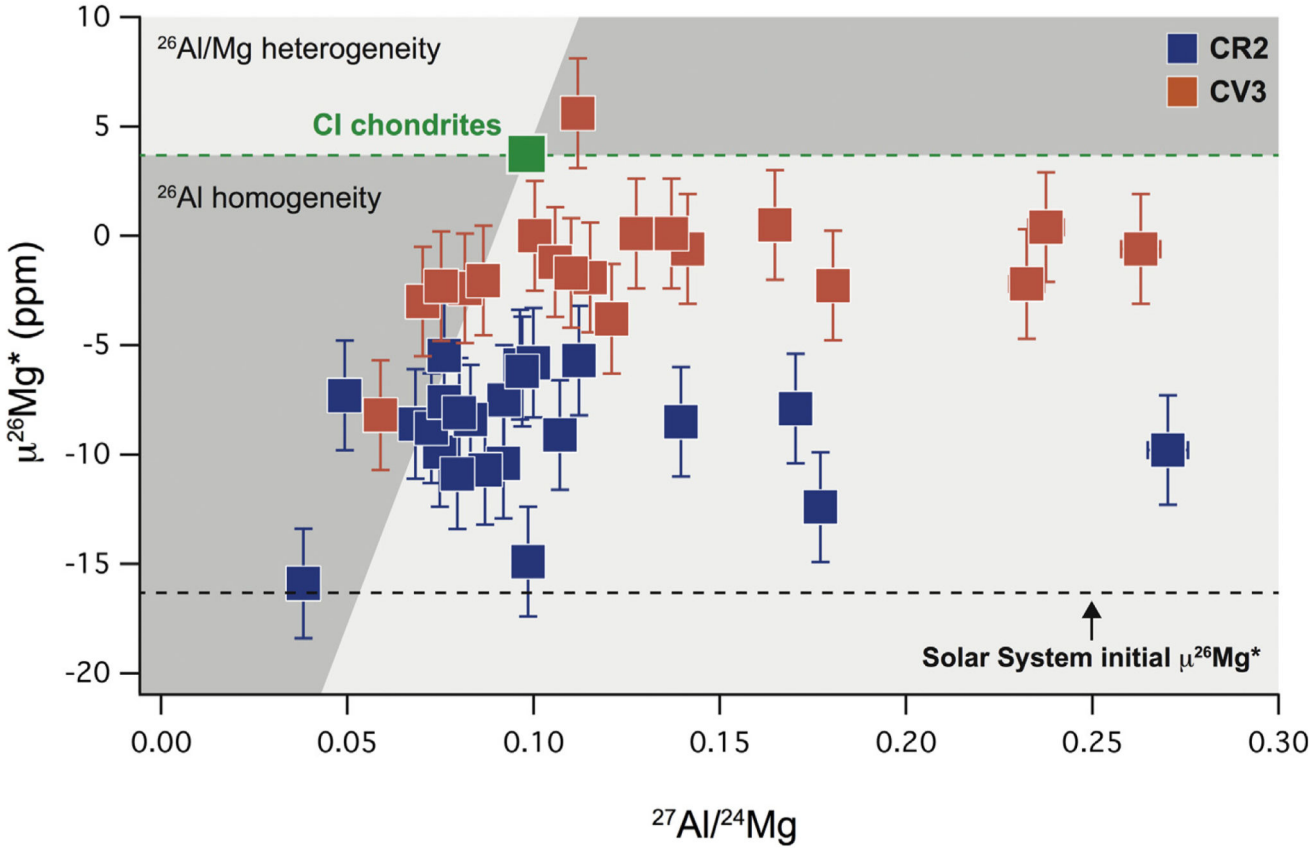

Fig. 5.

$\mu^{26}Mg^*$ and $^{27}Al/^{24}Mg$ variation diagram for chondrules from CV3 (red) and CR2 (blue) chondrites analyzed in this study. The ^{26}Al homogeneity field is based on the expected $\mu^{26}Mg^*$ composition of objects formed in a reservoir with an initial $^{26}Al/^{27}Al$ of $\sim 5 \times 10^{-5}$ and initial $\mu^{26}Mg^*$ value of –38 ppm, which reflects the total amount of radiogenic ingrowth in ^{26}Mg from the decay of ^{26}Al for a reservoir with solar Al/Mg (see Larsen et al., 2011 for more details on the model of ^{26}Al homogeneity). The depicted Solar System initial $\mu^{26}Mg^*$ composition of –15.9 ± 1.4 ppm and the bulk Solar System $\mu^{26}Mg^*$ value of 4.5 ± 1.1 ppm defined by CI chondrites are from Larsen et al. (2011). Note that the range of $\mu^{26}Mg^*$ values for the 42 chondrules is within that defined by the Solar System's initial and CI $\mu^{26}Mg^*$ compositions. Thus, the observed $\mu^{26}Mg^*$ variability for objects with near-solar Al/Mg values is in agreement with that predicted for ^{26}Al heterogeneity, which assumes that chondrules did not experience a complex history involving multiple Al/Mg fractionation events. Error bars reflect the external reproducibility of 2.5 ppm and 2% for the $\mu^{26}Mg^*$ and $^{27}Al/^{24}Mg$ values, respectively.

Europe PMC Funders Author Manuscripts

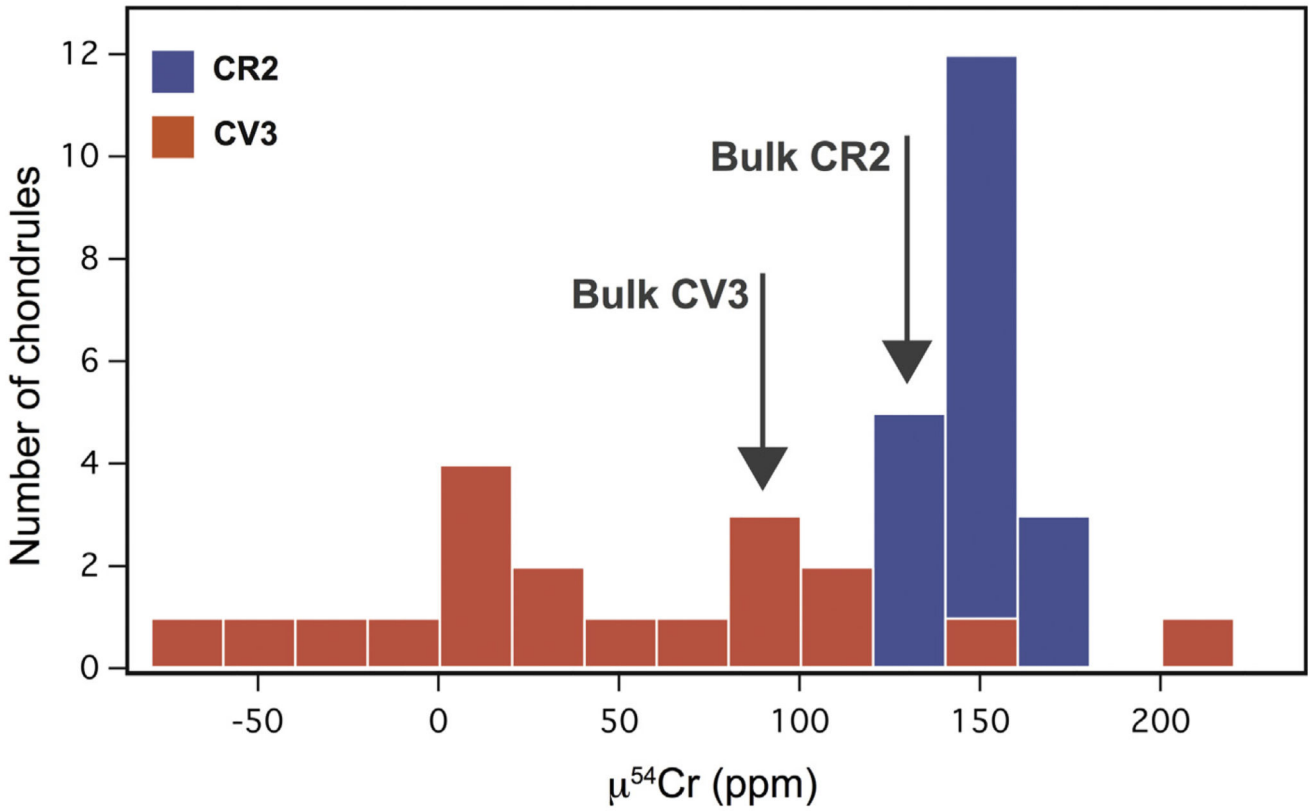

Fig. 6.

Histogram depicting the distribution of $\mu^{54}Cr$ values (ppm) for chondrules from CV3 (red) and CR2 (blue) chondrites analyzed in this study. Dataset include three additional chondrules from Allende from Connelly et al. (2012) and Trinquier et al. (2007). The chondrite bulk CV3 and CR2 estimates are from Trinquier et al. (2007). The range of $\mu^{54}Cr$ values recorded by CV3 chondrules is comparable to the compositional range defined by inner Solar System asteroidal and planetary bodies.

Europe PMC Funders Author Manuscripts

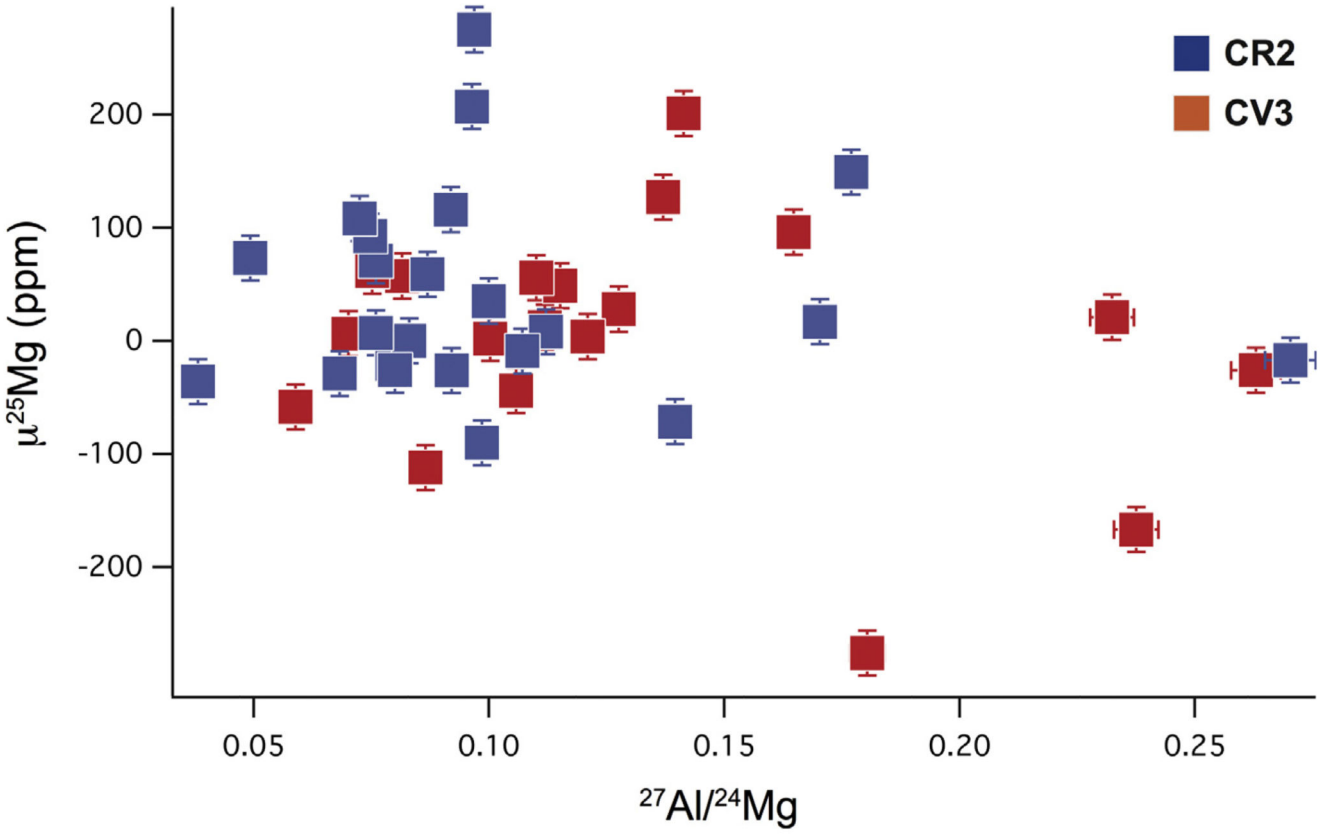

Fig. 7.

μ^{25}Mg (ppm) and $^{27}Al/^{24}Mg$ variation diagram for chondrules from CV3 (red) and CR2 (blue) chondrites analyzed in this study. The lack of positive correlation is not consistent with volatility-controlled processes as the main cause of the observed μ^{25}Mg variability in these chondrules. Error bars reflect the external reproducibility of 20 ppm and 2% for the μ^{25}Mg and $^{27}Al/^{24}Mg$ values, respectively.

Europe PMC Funders Author Manuscripts

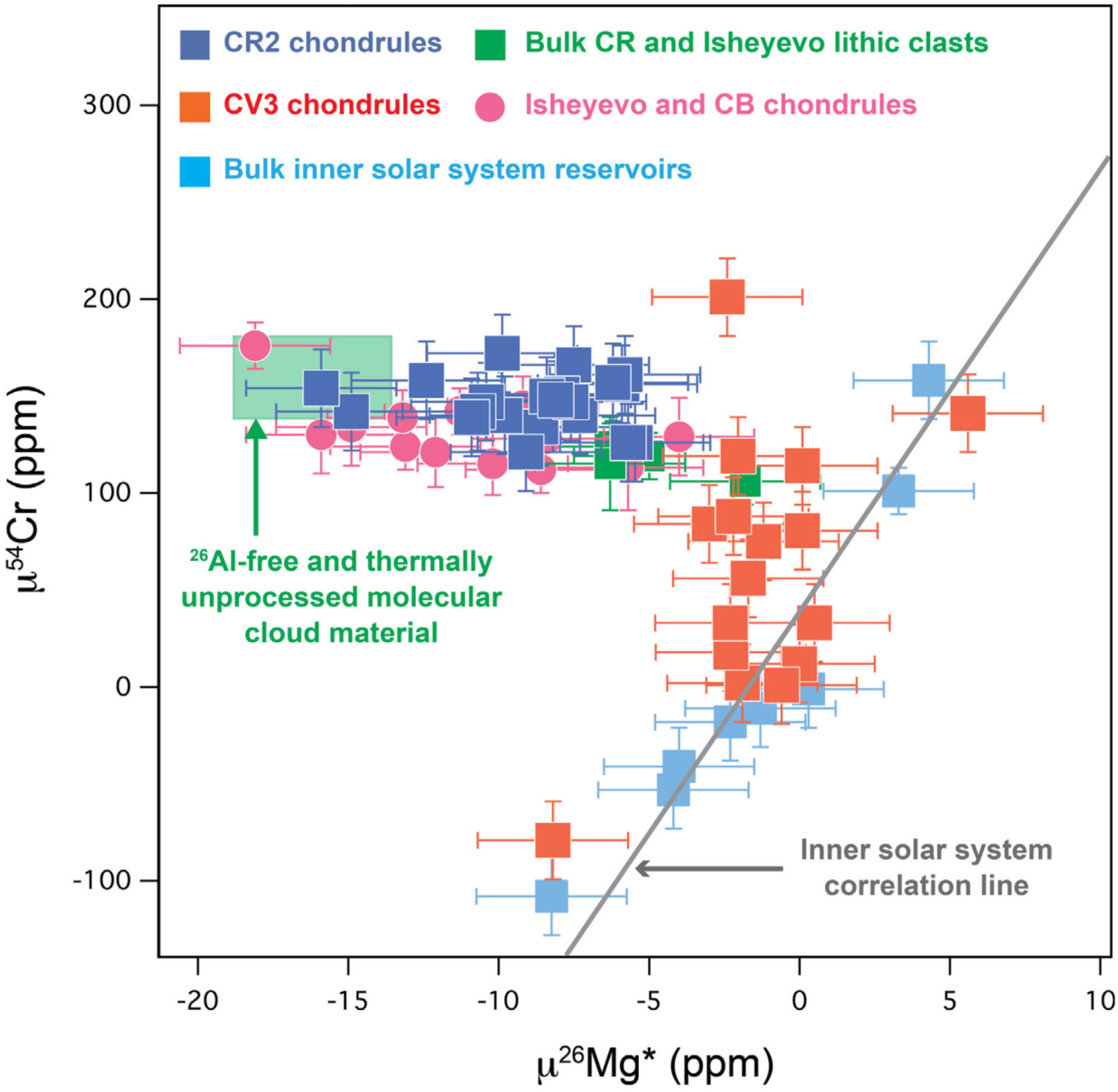

Fig. 8.

$\mu^{26}Mg^*$ (ppm) and $\mu^{54}Cr$ (ppm) variation diagram for chondrules from CV3 (red) and CR2 (blue) chondrites analyzed in this study, including CR chondrules previously reported by Van Kooten et al. (2016). Data for Isheyevo components, and bulk CR chondrites are from Van Kooten et al. (2016), Olsen et al. (2013) and Yamashita et al. (2010). The $\mu^{54}Cr$ and $\mu^{26}Mg^*$ compositions of the ^{26}Al-free and thermally-unprocessed molecular cloud material (green box), including their uncertainties, are defined by CI chondrites and the initial $\mu^{26}Mg^*$ value of the Solar System (Trinquier et al., 2007; Larsen et al., 2011). The inner

Solar System correlation line is defined by bulk inner Solar System reservoirs, including the composition of the CAI-forming gas (Larsen et al., 2011; Van Kooten et al., 2016).

Europe PMC Funders Author Manuscripts

Europe PMC Funders Author Manuscripts

Table 1

μ^{25}Mg and μ^{26}Mg* values of the USGS BHVO-2 and DTS-2b terrestrial rock standards analyzed in the course of this study.

Rock samples	μ^{25}Mg	2SE	μ^{26}Mg*	2SE	Reference standard	Source
BHVO-2 (1)	−107	4	−0.5	2.1	DSM-3	This study
DTS-2b (1)	−120	6	1.2	1.5	DSM-3	This study
DTS-2b	−117	19	−0.5	1.4	DSM-3	Olsen et al. (2013)
DTS-2b	−122	17	0.9	1.7	DSM-3	Bizzarro et al. (2011)
BHVO-2 (2)	−4	16	−1.0	2.3	DTS-2	This study
BHVO-2 (3)	−4	4	−2.8	2.2	DTS-2	This study
BHVO-2 (4)	−4	20	−1.7	1.5	DTS-2	This study
DTS-2b (2)	−18	21	−1.0	1.9	DTS-2	This study
DTS-2b (3)	−5	16	−0.4	1.6	DTS-2	This study

Table 2

Description of major petrological characteristics of chondrules investigated in this study.

Chondrule	Size (mm)	Type	Texture	Fo	Sub-Ca px	High-Ca px	Spinel	Metal	Rim	Alteration
Vigarano (CV3)										
V1	2.0	IAB	POP	96.4	$En_{96.7}$,$Wo_{0.6}$, $Fs_{2.7}$	$En_{53.4}$,$Wo_{42.0}$, $Fs_{4.6}$			Igneous	Light
V2	3.0	IA	BOP	95.8	$En_{70.4}$,$Wo_{0.5}$, $Fs_{29.1}$	$En_{37.5}$,$Wo_{42.6}$, $Fs_{19.9}$	x		Non	Intermediate
V3	2.0	IA	POP	89.8	$En_{92.9}$,$Wo_{6.0}$, $Fs_{1.0}$	$En_{50.0}$,$Wo_{46.4}$, $Fs_{3.6}$			FG	Moderate
V4	2.0	IA	POP	96.3					FG	Moderate
V6	1.5	IAB	POP Al-rich	98.3			x		Non	Light
V7	2.5	IAB	POP	94.9					FG	Intermediate
V9	1.5	IA	POP	97.4	$En_{75.0}$,$Wo_{4.4}$, $Fs_{20.5}$	$En_{65.4}$,$Wo_{3.5}$, $Fs_{3.5}$			FG	Moderate
V11	2.0	IAB	BOP	90.5			x		Igneous	Light
V12	3.0	IAB	POP	97.3					Non	Light
V15	3.0	IAB	POP px-rich	96.1	$En_{82.1}$,$Wo_{3.5}$, $Fs_{14.4}$				Igneous	Light
NWA 3118 (CV3)										
CV1	2.0	IAB	Compound BO	98.2					Igneous	Light
CV2	2.0	IAB	POP	95.7		$En_{59.2}$,$Wo_{38.1}$, $Fs_{2.7}$			FG	Intermediate
CV3	3.5	IAB	Compound BOP-POP	97.7			x		Igneous	Light
CV4	2.0	IAB	Compound BOP-POP	96.2					Igneous	Intermediate
CV5	1.5	IAB	BOP	94.1					Igneous	Light
CV6	1.0	IA	POP	94.5					FG	Moderate
CV9	1.5	IA	PO	98.0					FG	Intermediate
CV10	1.5	IAB	POP	91.6		$En_{53.2}$,$Wo_{45.4}$, $Fs_{1.4}$			Igneous	Moderate
CV11	2.0	IAB	POP	98.1					FG	Moderate
NWA 6043 (CR2)										
CR4	2.0	IA	POP	95.0					Non	Intermediate
CR5	2.0	IAB	BOP	95.7	$En_{93.9}$,$Wo_{2.3}$, $Fs_{3.8}$	$En_{47.8}$,$Wo_{36.3}$, $Fs_{15.8}$			2 × igneous	Light
CR6	1.0	IAB	BOP	98.9					Igneous	Light
CR7	2.0	IAB	POP	94.6	$En_{84.0}$,$Wo_{4.2}$, $Fs_{11.8}$	$En_{55.2}$,$Wo_{33.5}$, $Fs_{11.2}$	x		Non	Light
CR9	2.0	IAB	POP	93.2					Non	Intermediate
CR10	2.5	IAB	POP	97.6					Non	Light
CR11	1.5	IA	POP	92.5	$En_{85.0}$,$Wo_{6.4}$, $Fs_{8.6}$			x	Non	Light
CR12	2.0	IAB	POP	97.6	$En_{86.5}$,$Wo_{9.6}$, $Fs_{3.9}$			x	Non	Moderate
CR13	2.0	IA	POP	95.3		$En_{53.8}$,$Wo_{40.1}$, $Fs_{6.1}$		x	Non	Moderate
CR15	2.5	IAB	POP	97.2					Non	Intermediate
NWA 801 (CR2)										
MUS1	1.0	IA	POP	96.6				x	Non	Light
MUS2	2.0	IAB	POP	96.9				x	Non	Moderate
MUS3	1.5	IA	POP	95.2		$En_{55.0}$,$Wo_{39.7}$, $Fs_{5.2}$			Non	Light
MUS4	1.5	IAB	POP	96.1				x	Non	Intermediate
MUS5	3.0	IAB	BOP	97.1					Igneous	Moderate

Europe PMC Funders Author Manuscripts

Chondrule	Size (mm)	Type	Texture	Fo	Sub-Ca px	High-Ca px	Spinel	Metal	Rim	Alteration
MUS10	2.0	IAB	POP	94.1				x	Non	Intermediate
MUS11	2.0	IAB	POP	98.5				x	Igneous	Light
MUS12	2.5	IAB	POP	97.3				x	Non	Light
MUS13	1.5	IA	POP	95.3				x	Non	Moderate
MUS14	1.5	IAB	POP	95.9				x	Non	Intermediate
LAP 02342 (CR2)										
LAP1	1.5	IA	POP	98.3					FG	Moderate
LAP2	1.0	IA	POP	96.6				x	Non	Moderate
LAP3	1.0	IAB	POP	95.4				x	Igneous	Intermediate

Europe PMC Funders Author Manuscripts

Table 3

Major element composition of olivines from the chondrules investigated in this study. Fa, fayalite content. *N*, number of analyses.

	SiO_2	TiO_2	Al_2O_3	Cr_2O_3	FeO	MnO	MgO	CaO	Total	Fa	*N*
Vigarano (CV3)											
V1	44.84	0.07	0.38	0.34	8.53	0.17	44.67	0.36	99.36	2.8	26
V2	46.79	0.07	0.36	0.32	3.31	0,13	48.05	0.23	99.26	3.7	6
V3	41.17	0.08	0.27	0.53	9.28	0,16	48.04	0.24	99.77	9.7	26
V4	50.03	0.08	0.53	0.59	2.39	0,19	45.08	0.37	99.26	2.9	19
V6	41.68	0.08	0.18	0.40	1.37	0,13	54.55	0.19	98.58	1.4	7
V7	47.91	0.11	0.62	1.54	3.48	0,06	44.21	0.52	98.45	4.2	2
V9	45.07	0.08	0.32	0.25	1.80	0,06	50.46	0.43	98.47	2.0	16
V11	42.08	0.07	0.72	0.54	8.16	0,23	47.29	0.35	99.44	8.8	17
V12	42.85	0.06	0.19	0.29	2.15	0,07	52.48	0.33	98.42	2.2	20
V15	50.79	0.05	0.28	0.41	2.75	0,23	45.17	0.20	99.88	3.3	16
NWA 3118 (CV3)											
CV1	42.20	0.05	0.10	0.12	1.27	0.04	55.70	0.37	99.85	1.3	10
CV2	41.18	0.07	0.21	0.19	3.74	0.06	53.52	0.37	99.34	3.8	13
CV3	41.84	0.11	0.14	0.15	1.83	0.05	54.44	0.36	98.92	1.8	9
CV4	45.64	0.09	0.27	0.26	3.15	0.08	50.28	0.25	100.02	3.4	17
CV5	43.30	0.05	0.14	0.24	5.05	0.38	50.89	0.20	100.25	5.2	8
CV6	42.92	0.06	0.22	0.26	4.74	0.20	51.21	0.31	99.92	4.9	19
CV9	42.31	0.07	0.12	0.18	1.54	0.07	55.05	0.31	99.65	1.5	7
CV10	42.38	0.03	0.17	0.20	7.58	0.24	49.26	0.18	100.04	7.9	8
CV11	42.16	0.08	0.14	0.22	1.44	0.08	55.30	0.31	99.73	1.4	10
NWA 6043 (CR2)											
CR4	56.40	0.05	0.42	0.67	3.02	0.25	38.53	0.27	99.61	4.2	9
CR5	50.68	0.17	0.77	0.65	2.46	0.14	44.30	0.76	99.93	3.0	20
CR6	41.56	0.04	0.07	0.18	0.91	0.03	56.92	0.15	99.86	0.9	6
CR7	51.36	0.03	0.18	0.64	3.89	0.26	43.05	0.20	99.61	4.8	9
CR9	46.79	0.05	0.34	0.73	5.31	0.33	46.29	0.30	100.14	6.0	12
CR10	40.53	0.01	0.08	0.26	1.93	0.06	57.68	0.41	100.96	1.8	2
CR11	54.20	0.11	0.76	0.82	4.67	0.28	37.96	0.41	99.21	6.4	4
CR12	48.71	0.10	0.47	0.54	1.48	0.09	47.98	0.45	99.82	1.7	22
CR13	49.87	0.06	0.39	0.62	3.26	0.20	44.53	0.33	99.26	3.9	15
CR15	48.97	0.11	0.66	0.49	1.65	0.10	47.21	0.52	99.71	1.9	10
NWA 801 (CR2)											
MUS1	46.31	0.04	0.22	0.64	2.68	0.09	49.51	0.29	99.78	2.9	14
MUS2	42.03	0.03	0.74	0.53	2.06	0.09	52.79	0.64	98.91	2.1	9
MUS3	41.62	0.01	0.04	0.60	4.20	0.27	52.21	0.19	99.14	4.3	5
MUS4	53.57	0.10	0.68	0.83	2.16	0.18	41.64	0.50	99.66	2.8	9

Europe PMC Funders Author Manuscripts

	SiO_2	TiO_2	Al_2O_3	Cr_2O_3	FeO	MnO	MgO	CaO	Total	Fa	*N*
MUS5	41.01	0.03	0.06	0.51	2.07	0.33	52.14	0.32	96.47	2.2	1
MUS10	40.96	0.02	0.03	0.66	4.89	0.67	51.01	0.14	98.38	5.1	5
MUS11	41.56	0.00	0.11	0.20	0.97	0.00	54.80	0.38	98.02	1.0	1
MUS12	41.06	0.01	0.10	0.29	2.28	0.08	54.02	0.22	98.06	2.3	2
MUS13	57.89	0.09	0.51	0.76	2.46	0.27	35.75	0.35	98.08	3.7	1
MUS14	41.22	0.01	0.09	0.63	3.52	0.16	52.34	0.21	98.18	3.6	4
LAP 02342 (CR2)											
LAP1	42.27	0.05	0.21	0.25	1.12	0.04	55.67	0.44	100.05	1.1	8
LAP2	44.84	0.04	0.12	0.65	2.87	0.18	51.80	0.19	100.69	3.0	10
LAP3	45.88	0.09	0.42	0.81	3.44	0.22	49.36	0.45	100.67	3.7	17

Table 4

Major element composition of pyroxenes from selected chondrules investigated in this study. Fa, fayalite content. *N*, number of analyses.

	SiO_2	TiO_2	Al_2O_3	Cr_2O_3	FeO	MnO	MgO	CaO	Na_2O	Total	Wo	En	Fs	*N*
Vigarano (CV3)														
V1 Sub-Ca px	46.77	0.10	0.51	0.70	2.40	0.24	48.09	0.40	0.01	99.22	0.6	96.7	2.7	3
V1 high-Ca px	50.31	0.68	13.73	1.07	2.21	0.26	14.42	15.78	0.91	99.37	42.0	53.4	4.6	4
V2 Sub-Ca px	37.47	0.03	0.05	0.18	26.06	0.22	35.35	0.32	0.02	99.70	0.5	70.4	29.1	4
V2 high-Ca px	47.20	0.62	16.34	0.47	8.97	0.15	9.49	14.99	0.57	98.80	42.6	37.5	19.9	2
V3 Sub-Ca px	57.36	0.52	2.52	0.75	0.70	0.16	34.77	3.13	0.05	99.96	6.0	92.9	1.0	1
V3 high-Ca px	50.44	0.91	14.67	0.68	1.64	0.25	12.64	16.32	1.88	99.43	46.4	50.0	3.6	6
V9 Sub-Ca px	49.33	0.13	2.68	0.56	14.47	0.34	29.64	2.45	0.18	99.78	4.4	75.0	20.5	3
V9 high-Ca px	52.76	0.59	2.64	1.01	2.26	0.53	23.56	15.60	0.10	99.05	31.1	65.4	3.5	3
V15 Sub-Ca px	44.56	0.18	1.23	0.73	12.03	0.25	38.43	2.26	0.00	99.67	3.5	82.1	14.4	2
NWA 3118 (CV3)														
CV2 high-Ca px	50.88	0.71	6.13	2.78	1.59	1.00	19.53	17.49	0.09	100.20	38.1	59.2	2.7	1
CV10 high-Ca-px	48.81	1.10	8.50	1.94	0.83	0.28	17.44	20.68	0.01	99.59	45.4	53.2	1.4	2
NWA 6043 (CR2)														
CR5 Sub-Ca px	47.75	0.16	0.91	0.69	3.21	0.08	44.46	1.54	0.01	98.81	2.3	93.9	3.8	2
CR5 High-Ca px	46.60	0.92	6.97	0.78	9.29	0.13	15.74	16.64	0.15	97.22	36.3	47.8	15.8	5
CR7 Sub-Ca px	53.50	0.14	1.50	1.29	7.75	0.62	30.85	2.15	0.07	97.87	4.2	84.0	11.8	4
CR7 High-Ca px	48.04	0.61	5.86	2.27	6.70	0.89	18.47	15.61	0.13	98.58	33.5	55.2	11.2	20
CR11 Sub-Ca px	41.58	0.31	3.11	1.01	7.39	0.39	41.01	4.27	0.10	99.17	6.4	85.0	8.6	2
CR12 Sub-Ca px	55.47	0.30	2.82	1.11	2.55	0.22	31.86	4.92	0.00	99.25	9.6	86.5	3.9	3
CR13 High-Ca px	47.80	0.86	7.92	2.31	3.49	0.55	17.35	18.00	0.08	98.36	40.1	53.8	6.1	10
NWA 801 (CR2)														
MUS 3 High-Ca px	48.23	0.80	8.20	2.37	2.93	0.82	17.24	17.32	0.08	97.99	39.7	55.0	5.2	5

Europe PMC Funders Author Manuscripts

Table 5

Major element composition of mesostasis from selected chondrules investigated in this study. *N*, number of analyses.

	SiO_2	TiO_2	Al_2O_3	Cr_2O_3	FeO	MnO	MgO	CaO	Na_2O	Total	*N*
Vigarano(CV3)											
V1	52.18	0.60	20.77	0.47	1.84	0.30	6.32	14.47	1.81	98.77	6
V3	50.56	0.70	18.52	0.46	2.96	0.12	7.68	10.40	5.52	96.92	9
V6	45.08	1.16	20.76	0.10	1.53	0.04	10.28	18.40	1.06	98.40	2
V11	43.49	0.42	30.82	0.08	0.37	0.01	2.27	19.59	0.76	97.82	5
NWA 3118 (CV3)											
CV5	43.64	0.06	33.64	0.01	0.14	0.00	2.26	19.14	0.04	98.92	3
NWA 6043 (CR2)											
CR5	49.15	0.42	15.09	0.48	2.74	0.09	20.96	10.52	0.41	99.85	9
CR6	56.34	0.81	20.01	0.26	0.91	0.03	4.41	17.09	0.58	100.45	3
RC7	53.01	0.53	21.53	0.31	3.21	0.62	5.52	12.70	2.26	99.68	13
CR9	49.97	0.87	11.51	1.49	4.26	0.61	15.21	16.04	0.33	100.27	7
CR10	47.64	1.11	18.92	0.74	3.34	0.12	10.50	15.54	0.70	98.60	2
CR12	48.62	0.44	17.37	0.55	2.26	0.10	13.24	15.11	0.50	98.18	11
CR13	52.11	0.49	22.54	0.31	2.73	0.30	5.57	13.43	1.59	99.09	9

Table 6

$^{27}Al/^{24}Mg$, $\mu^{25}Mg$, $\mu^{26}Mg^*$ and $\mu^{54}Cr$ values for chondrules investigated in this study.

	$^{27}Al/^{24}Mg$	$\mu^{25}Mg$	2SE	$\mu^{26}Mg^*$	2SE	$\mu^{54}Cr$	2SE
Vigarano (CV3)							
V1	0.12	49	10	−1.9	1.4	2	20
V2	0.13	28	3	0.1	1.9	114	20
V3	0.08	57	3	−2.4	1.6	201	13
V4	0.10	2	2	0.0	1.5	12	10
V6	0.16	96	15	0.5	1.9	33	20
V7	0.14	201	31	−0.6	0.8	1	14
V9	0.07	6	3	−3.0	2.0	84	11
V11	0.18	−276	15	−2.3	0.6	18	2
V12	0.11	12	13	5.6	1.7	141	17
V15	0.06	−58	9	−8.2	1.6	−79	10
NWA 3118 (CV3)							
CV1	0.24	−167	19	0.4	2.2		
CV2	0.11	−44	16	−1.2	1.2	75	10
CV3	0.23	21	13	−2.2	1.4	88	15
CV4	0.12	4	9	−3.8	1.7		
CV5	0.26	−26	9	−0.6	1.2		
CV6	0.08	61	8	−2.3	1.5	33	11
CV9	0.11	56	7	−1.7	1.8	56	8
CV10	0.14	127	16	0.1	1.4	81	10
CV11	0.09	−112	11	−2.0	1.0	119	12
NWA 6043 (CR2)							
CR4	0.07	−29	39	−8.6	1.5	134	6
CR5	0.27	−17	3	−9.8	1.4		
CR6	0.14	−72	4	−8.5	1.4		
CR7	0.09	−26	4	−7.5	1.1	166	8
CR9	0.08	71	7	−5.5	0.8	129	8
CR10	0.10	−90	4	−14.9	1.0	142	11
CR11	0.07	92	5	−9.9	0.8	172	7
CR12	0.09	116	11	−10.4	0.9	147	7
CR13	0.09	59	6	−10.7	2.8	142	6
CR15	0.05	73	5	−7.3	1.5	140	6
NWA 801 (CR2)							
MUS1	0.08	−21	4	−10.9	1.4	139	11
MUS2	0.10	207	10	−5.9	2.0	156	15
MUS3	0.10	35	16	−5.8	1.8	161	11
MUS4	0.17	17	16	−7.9	1.6	151	9
MUS5	0.11	8	12	−5.7	2.5	126	9

Europe PMC Funders Author Manuscripts

	$^{27}Al/^{24}Mg$	$\mu^{25}Mg$	2SE	$\mu^{26}Mg^{*}$	2SE	$\mu^{54}Cr$	2SE
MUS10	0.08	0	15	−8.4	1.8	150	20
MUS11	0.11	−9	14	−9.1	1.8	121	7
MUS12	0.07	108	13	−8.8	2.1		
MUS13	0.08	7	12	−7.6	1.8	147	6
MUS14	0.10	275	16	−6.2	1.7	157	8
LAP 02342 (CR2)							
LAP1	0.04	−36	21	−15.9	1.9	154	15
LAP2	0.08	−26	19	−8.1	1.8	148	6
LAP3	0.18	149	6	−12.4	1.0	158	10

Europe PMC Funders Author Manuscripts

Table 7

Model initial $^{26}Al/^{27}Al$ of chondrule precursors for objects with near solar $^{27}Al/^{24}Mg$ ratios (±10%). Uncertainties in the model initial $^{26}Al/^{27}Al$ reflect the external reproducibility of 2,5 ppm on the measured $\mu^{26}Mg^*$ values combined with the uncertainties of the initial Solar System estimate (Larsen et al., 2011).

Chondrule	$^{27}Al/^{24}Mg$	$\mu^{26}Mg^*$ (ppm)	Model $[^{26}Al/^{27}Al]_0$
V4	0.10	0.0	$(2.2 \pm 0.4)\times10^{-5}$
CV2	0.11	−1.2	$(2.1 \pm 0.4)\times10^{-}5$
CV9	0.11	−1.7	$(2.0 \pm 0.4)\times10^{-5}$
CR7	0.09	−7.5	$(1.3 \pm 0.4)\times10^{-5}$
CR10	0.10	−14.9	$(1.5 \pm 4.0)\times10^{-6}$
CR12	0.09	−10.4	$(8.7 \pm 4.4)\times10^{-6}$
MUS2	0.10	−5.9	$(1.4 \pm 0.4)\times10^{-5}$
MUS3	0.10	−5.8	$(1.4 \pm 0.4)\times10^{-5}$
MUS11	0.11	−9.1	$(8.7 \pm 3.6)\times10^{-6}$
MUS14	0.10	−6.2	$(1.4 \pm 0.4)\times10^{-5}$